

**Intrinsic structural instabilities of domain walls driven by gradient couplings:
meandering antiferrodistortive-ferroelectric domain walls in BiFeO₃**

Eugene A. Eliseev¹, Anna N. Morozovska², Christopher T. Nelson³, and Sergei V. Kalinin^{3}*

¹ *Institute for Problems of Materials Science, National Academy of Sciences of Ukraine,
Krjijanovskogo 3, 03142 Kyiv, Ukraine*

² *Institute of Physics, National Academy of Sciences of Ukraine,
46, pr. Nauky, 03028 Kyiv, Ukraine*

³ *The Center for Nanophase Materials Sciences, Oak Ridge National Laboratory,
Oak Ridge, TN 37831*

Abstract

Using Landau-Ginzburg-Devonshire approach, we predict the intrinsic instability of the ferroelectric-ferroelastic domain walls in the multiferroic BiFeO₃ emerging from the interplay between the AFD and FE gradient terms at the interfaces. These instabilities are the interface analogue of the structural instabilities in the vicinity of phase coexistence in the bulk; and so they do not stem from either incomplete polarization screening in thin films or its spatial confinement, electrostrictive or flexoelectric coupling. The effect of BiFeO₃ material parameters on the 71–, 109–, and 180– degree walls is explored, and it is shown that the meandering instability appears at 109–, and 180– degree walls for small gradient energies, and the walls become straight and broaden for higher gradients. In contrast to the 180– and 109 – degree domain walls, uncharged 71-degree AFD-FE walls are always straight, but their width increase with the tilt gradient coefficient increase. This fundamental wall instability and associated intrinsic meandering provides a new insight into behaviors of morphotropic and relaxor materials, wall pinning, and mechanisms of interactions between order parameter fields and local microstructure.

* corresponding author, e-mail: sergei2@ornl.gov

I. INTRODUCTION

Multiferroics, defined as materials with more than one ferroic [1] long-range orders, are ideal systems for fundamental studies of couplings among the order parameters of different nature, e.g. ferroelectric (**FE**) polarization, structural antiferrodistortion (**AFD**), ferromagnetic (**FM**) and antiferromagnetic (**AFM**) order parameters [2, 3, 4, 5, 6, 7, 8, 9]. The AFD, FE, FM, and AFM degrees of freedom in multiferroics are interlinked via different types of biquadratic couplings leading to versatile phase diagrams and complex domain structures [2-9]. In many cases, the interaction of the versatile domain structures with underpinning frozen disorder gives rise to highly mobile structures and materials with giant functional responses.

The biquadratic couplings between AFD and other long-range orders are universal for all multiferroics with rotational antiferrodistortive symmetry [10]. The most common is "rotoelectric" Houchmandazeh-Laizerowicz-Salje coupling, that is the biquadratic coupling between the AFD order parameter and polarization [11, 12] that can significantly influence the structure and local properties of domain walls in AFD multiferroics [13, 14]. Similarly, the biquadratic magnetoelectric coupling, that is the coupling between polarization and magnetization [2, 3], can influence phase diagrams, domain wall structure and morphology [15]. The bilinear flexoelectric coupling [16], that coupled the strain gradient with polarization and vice versa, can induce incommensurate spatially modulated phases in ferroics including antiferroelectric (**AFE**) and AFD ones [17, 18, 19, 20]. The flexo-antiferrodistortive coupling, inherent to all AFD systems, can lead to the formation of incommensurate, spatially-modulated AFD and AFE phases in multiferroics [21], which are indeed observed in e.g. $\text{Bi}_y\text{Sm}_{1-y}\text{FeO}_3$ [17], EuTiO_3 [22, 23]. There are also a wide variety of spatially modulated domain structures observed experimentally at the morphotropic boundaries in multiferroics [24, 25, 26, 27, 28], which are sometimes identified as monoclinic phase regions by scattering.

The vector nature of the AFD order parameter can strongly influence the phase stability, domain structure, polar, dielectric and magnetoelectric properties of (multi)ferroic thin films [29, 30, 31]. Sometimes phase diagrams of thin (strained) films are complicated by unusual low symmetry phases, which are absent in their bulk counterparts [32, 33, 34, 35]. Vortices and vertices composed by the closure of domain walls have been observed experimentally in nanoscale multiferroics [36, 37], especially in BFO [38, 39]. Surface-induced labyrinthine domain structures were observed in ergodic relaxors and explained by the presence of higher-order term in free-energy expansion that gives rise to the polarization modulations. Fractal domain structures have been observed in multiferroic thin films [40], near the surface of ferroelectric relaxors close to relaxor-ferroelectric transition [41].

The labyrinthine domain structures, which can coexist with classical ferroelectric domains closer to ferroelectric composition limit, have been observed in ergodic relaxors [42, 43] [44]. The labyrinthine domain structure was predicted theoretically in thin films of incommensurate and bilayered ferroelectrics [45, 46], being similar to those observed in ultrathin magnetic films [47]. Spherical nanoparticles of uniaxial ferroelectrics CuInP_2S_6 and $\text{Sn}_2\text{P}_2\text{S}_6$ covered by a layer of screening charge with finite screening length revealed the transformation from a regular stripe domain structure into a labyrinth pattern when the gradient term decreases below the critical value [48, 49]. The transition can be identified as a gradient-induced morphological transition, and appeared unrelated with flexoelectric or electrostrictive, or any other bilinear, or biquadratic couplings influence.

To the best of our knowledge the physical origin of complex morphology of domain structures and low symmetry modulated phases in nanoscale ferroics is the imbalance between domain wall surface energy and electric or magnetic (or possibly elastic) field energy contributions. Specifically, a ferroelectric nanoparticle tends to minimize its electric energy by creation of the complex or/and irregular features of domain structure near the free surfaces, but the structure cannot be too fine-scale due to the increasing energy of domain walls (see e.g. discussion in Refs.[48-49]). Much more complex situation (corresponding to the balance of labyrinthine domains in the bulk and vortices at the surface) are expected in multiaxial ferroelectrics with polarization rotation allowed, such as BaTiO_3 , $(\text{Pb,Zr})\text{TiO}_3$ and BiFeO_3 , and the fundamental question about the instability threshold of regular domain structure in nanoscale multiaxial multiferroics remains open.

The gap in the knowledge motivates this work that reveals a low symmetry meandering zig-zag like instability of AFD-FE domain walls in thin BFO films. This unexpected result, obtained by finite element modeling (**FEM**), is explained within LGD-theory framework.

The original part of the manuscript is structured as follows. LGD free energy are listed and described in **section II.A**. The problem statement including the problem geometry, brief form of coupled Euler-Lagrange equations with boundary conditions are discussed in **section II.B**. The impact of biquadratic coupling on the stability of homogeneous phases is analyzed in **section II.C**. Simulation details with the special attention to the measures taken to establish the physical origin of complex domain morphologies are described in **section III.A**. The appearance of low symmetry phases limited by 180-degree or 109-degree meandering zig-zag AFD-FE domains and their changes with the gradient energy increase are presented in **section III.B** and **III.C**, respectively. The gradient-driven broadening of AFD-FE 71-degree domain walls is discussed in **section III.D**. **Section IV** is a brief summary. Evident form of the free energy, boundary conditions and material parameters are given in **Appendix A**.

II. THEORETICAL FORMALISM

As a model system, we have chosen BFO solid solutions. Pristine and rare-earth doped bismuth ferrite BiFeO_3 (**BFO**) is the unique multiferroic [50, 51] with a strong FE polarization, structural rotational AFD, FM and AFM long-range orders coexisting up to room and elevated temperatures. Specifically bulk BFO exhibits AFD long-range order at temperatures below 1200 K; it is FE with a large spontaneous polarization below 1100 K and is AFM below Neel temperature $T_N \approx 650$ K [52]. Notably that the behaviour of the structural order parameter at the domain walls of BFO determines their structure and energy [53]. Domain walls in BFO exhibit unusual electrophysical properties, such as conduction and magnetotransport enhancement [54, 55, 56, 57, 58, 59]. Recently, a complete phase diagram of BFO including the AFM, FE, and AFD phases was calculated within Landau-Ginzburg-Devonshire (**LGD**) theory [60].

The pronounced multiferroic properties and unusual domain structure evolution maintain in BFO thin films and heterostructures [61, 62, 63, 64, 65, 66, 67, 68, 69]. In particular, atomic mapping of structural distortions in 109-degree domains in BiFeO_3 thin films [70] revealed, that the coexistence of rhombohedral and orthorhombic phases in ultrathin BiFeO_3 films can be driven by interfacial oxygen octahedral coupling [71]. The role of the rotomagnetic coupling, that is the biquadratic coupling between the AFD and AFM (or FM) orders [72], has been studied in BFO fine grained ceramics [73].

A. Landau-Ginzburg-Devonshire free energy

Thermodynamic Landau-Ginzburg-Devonshire (**LGD**) potential G that describes antiferromagnetic (**AFM**), ferroelectric (**FE**) and antiferrodistortive (**AFD**) properties of BFO is:

$$G = \int_V (\Delta G_{AFD} + \Delta G_{FE} + \Delta G_{AFM} + \Delta G_{BQC} + \Delta G_{ELS}) dv + \int_S (\Delta G_{AFD} + \Delta G_{FE}) dS \quad (1)$$

The AFD energy in the "host" BFO lattice at room temperature, corresponding to $R3c$ phase, is a six-order expansion on the oxygen tilt Φ_i and its gradients,

$$\Delta G_{AFD} = b_i(T) \Phi_i^2 + b_{ij} \Phi_i^2 \Phi_j^2 + b_{ijk} \Phi_i^2 \Phi_j^2 \Phi_k^2 + v_{ijkl}^{(\Phi)} \frac{\partial \Phi_i}{\partial x_k} \frac{\partial \Phi_j}{\partial x_l}. \quad (2)$$

Here Φ_i are components of pseudovectors, determining out-of-phase static rotations of oxygen octahedral groups (eigenvectors of AFD modes of lattice vibrations), and Einstein summation convention is employed.

FE energy ΔG_{FE} is a six-order expansion on the polarization vector P_i and its gradients,

$$\Delta G_{FE} = a_i^{(P)} P_i^2 + a_{ij}^{(P)} P_i^2 P_j^2 + a_{ijk}^{(P)} P_i^2 P_j^2 P_k^2 + g_{ijkl}^{(P)} \frac{\partial P_i}{\partial x_k} \frac{\partial P_j}{\partial x_l}. \quad (3)$$

In accordance with the classical LGD theory, we assume that the coefficients b_i and $a_k^{(P)}$ are temperature dependent following Barrett law [74], $b_i = b_T T_{q\Phi} (\coth(T_{q\Phi}/T) - \coth(T_{q\Phi}/T_\Phi))$ and $a_k^{(P)} = \alpha_T (T_{qP} \coth(T_{qP}/T) - T_C)$, where T_Φ and T_C are corresponding virtual Curie temperatures, $T_{q\Phi}$ and T_{qP} are characteristic temperatures [75].

AFM energy ΔG_{AFM} is a fourth-order expansion in terms of the AFM order parameter vector L_i and its gradient, as follows from the fact that this phase transition in BFO is second order [60]. The details of ΔG_{AFM} is considered elsewhere [60].

The AFD-FE coupling energy ΔG_{BQC} is a biquadratic function of the order parameters polarization P_i and tilts Φ_i :

$$\Delta G_{BQC} = \zeta_{ijkl} \Phi_i \Phi_j P_k P_l. \quad (4)$$

For a given symmetry, the coupling energy in Eq. (5) includes unknown tensorial coefficients in Voight notations for the AFD-FE biquadratic couplings (ζ_{44} , ζ_{11} , ζ_{12}).

The elastic energy (without rotostriction coupling) is

$$\Delta G_{ELS} = -s_{ijkl} \sigma_{ij} \sigma_{kl} - Q_{ijkl} \sigma_{ij} P_k P_l - \frac{F_{ijkl}}{2} \left(\sigma_{ij} \frac{\partial P_k}{\partial x_l} - P_k \frac{\partial \sigma_{ij}}{\partial x_l} \right). \quad (5)$$

Here s_{ijkl} are elastic compliances tensor components, Q_{ijkl} are electrostriction tensor components, F_{ijkl} are flexoelectric tensor components.

The surface energy has the form:

$$\int_S (\Delta G_{AFD} + \Delta G_{FE}) dS = \int_S \left(\frac{b_i^{(S)}}{2} \Phi_i^2 + \frac{a_i^{(S)}}{2} P_i^2 \right) dS \quad (6)$$

Surface energy coefficients $b_i^{(S)}$ and $a_i^{(S)}$ have different nature and control the broadening at the surface of ADF and FE domain walls, respectively.

B. Problem statement

We consider a BFO film with thickness h placed in a perfect electric contact with conducting bottom electrode that mechanically clamps the film. The top surface of the film is mechanically free and can

be in an ideal electric contact with the top electrode, or electrically open, or covered with the surface screening charge with density $\sigma(\varphi)$ that's appear due to surface states [76], or electro-chemically active ions [77, 78, 79, 80] [see **Fig. 1, top**]. Bottom row in **Fig.1** shows three types (a)-(c) of nominally uncharged 180-, 109- and 71-degree domain walls in BFO.

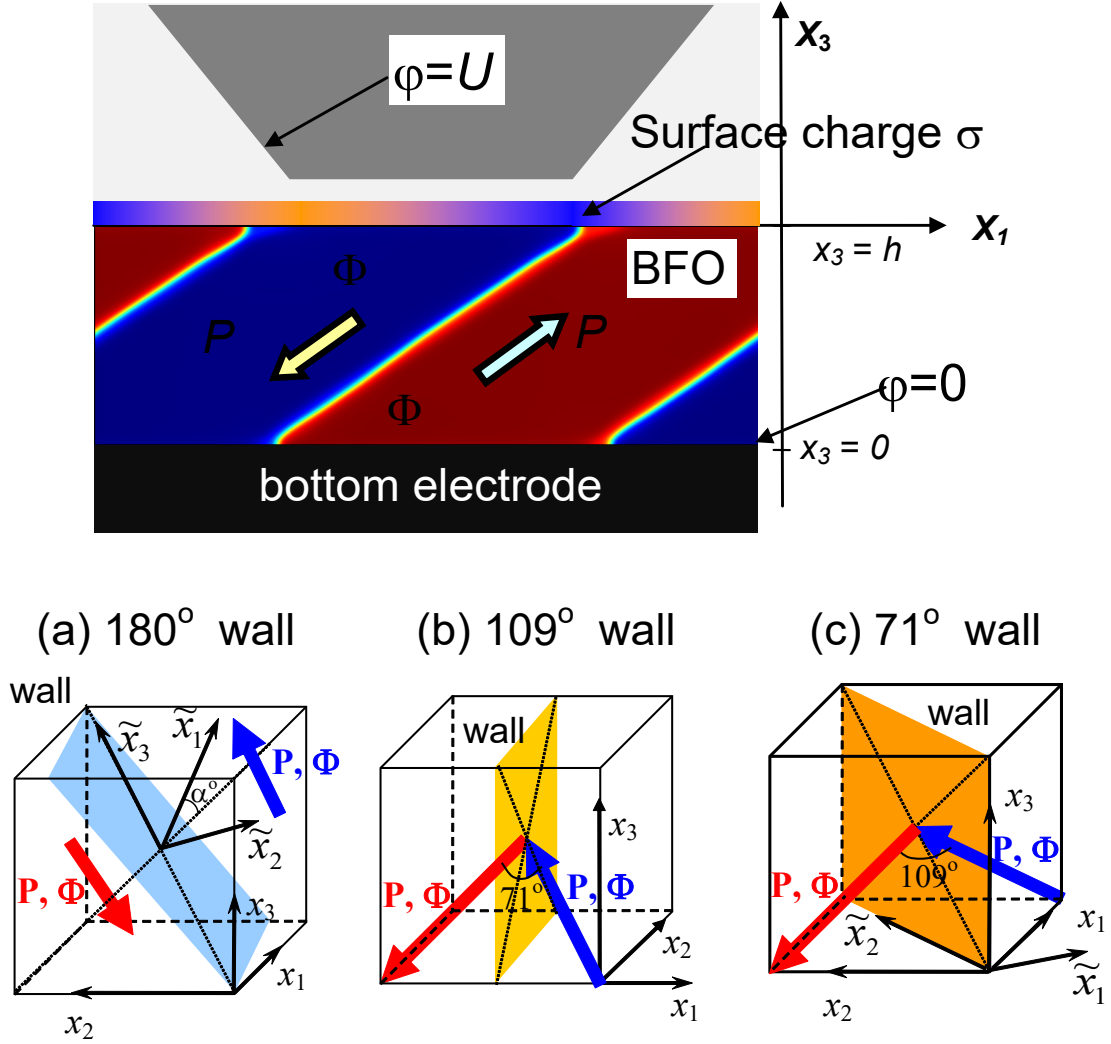


FIGURE. 1. Considered system, consisting of electrically conducting bottom electrode, BFO film of thickness h with a domain structure (if any exists), surface screening charge with density $\sigma(\varphi)$ (a model for imperfect screening) and ambient media (from bottom to the top). Three types of nominally uncharged 180- (a), 109- (b) and 71-degree (c) domain walls in BFO are shown in the bottom row.

Electric boundary conditions are the zero electric potential at the bottom of the film contacting the conducting substrate $\varphi|_{x_3=0} = 0$, and its continuity, $\varphi|_{x_3=h-0} - \varphi|_{x_3=h+0} = 0$, at the interface between the ferroelectric film and the ambient medium. Another boundary condition at the

latter interface requires the equivalence of a discontinuity in the normal component of the electric displacement to the surface free charge $\left(P_3 - \varepsilon_0 \varepsilon_b \frac{\partial \varphi}{\partial x_3} \right) \Big|_{x_3=h-0} + \varepsilon_0 \varepsilon_e \frac{\partial \varphi}{\partial x_3} \Big|_{x_3=h+0} + \sigma(\varphi) \Big|_{x_3=h} = 0$. Here, we consider the special case of the surface screening charge with the density given by $\sigma(\varphi) = -\varepsilon_0 \varphi / \Lambda$, where Λ is the effective screening length [81]. Typically the value of Λ is smaller or even significantly smaller [82, 83] than 1 nm. The condition $\Lambda \rightarrow 0$ corresponds to the perfect electric contact between the top electrode and the film, and we consider this limiting case for comparison. For the case the top electrode can be either biased ($\varphi|_{x_3=h} = U$) or grounded ($\varphi|_{x_3=h} = 0$), depending on the experimental situation corresponding to the SPM tip placed on the film surface.

Elastic problem formulation is based on the modified Hooke's law obtained using the thermodynamic relation $u_{ij} = -\frac{\delta G_{ELS}}{\delta \sigma_{kl}}$, where u_{ij} are elastic strain tensor components. Mechanical equilibrium conditions are $\partial \sigma_{ij} / \partial x_j = 0$ [84]. Note that the film-substrate interface was considered as unstrained one (misfit strain is zero) corresponding to the elastically matched substrate.

The coupled system of Euler-Lagrange equations allowing for Khalatnikov relaxation of the oxygen tilt and polarization components Φ_i and P_i is:

$$\frac{\delta G}{\delta P_i} = -\Gamma \frac{\partial P_i}{\partial t} \text{ and } \frac{\delta G}{\delta \Phi_i} = -\Gamma \frac{\partial \Phi_i}{\partial t}. \quad (7a)$$

These equations are supplemented by the boundary conditions of zero generalized fluxes at the film boundaries,

$$b^{(S)} \Phi_i + v_{ijkl}^{(\Phi)} \frac{\partial \Phi_j}{\partial x_k} n_l \Big|_S = 0, \quad a^{(P)} P_i + g_{ijkl}^{(P)} \frac{\partial P_j}{\partial x_k} n_l \Big|_S = 0 \quad (i=1, 2, 3). \quad (7b)$$

The boundary problem Eqs. (7a,b) was analyzed numerically using finite element modelling (**FEM**) for BFO films.

C. The impact of biquadratic coupling on the stability of homogeneous phases

Experimentally, bulk BFO should be in a rhombohedral R3c phase at temperatures below T_C . Since the biquadratic coupling, gradient energy and some other higher order coefficients in the free energy (1)-(5) are known only poorly, one should be very careful with the choice of their numerical values in order to prevent the appearance of so-called nonphysical "parasitic" phases [60], which do not exist in reality and can mislead the theoretical analyses of the domain structure configuration.

Therefore, before modeling the effect of gradient energy on domain structure, we analyze whether the parasitic phase can be (meta)stable below T_C for a chosen free energy functional form (1)-(5) allowing for the biquadratic coupling (4) for parameters listed in **Table I**. For this purpose let us perform the following analytical and numerical calculations.

Without biquadratic coupling contribution, i.e. for $\Delta G_{BQC} = 0$, and neglecting the 6-th powers of the polarizations and tilts, and their gradients, the energies of oxygen tilts and polarization are decoupled, and, using the idea of Dzyaloshinsky substitution [85], one can introduce the new variables $\Phi^2 = \frac{\Phi_1^2 + \Phi_2^2 + \Phi_3^2}{\sqrt{3}}$, $\Psi^2 = \frac{\Phi_3^2 - \Phi_1^2}{\sqrt{2}}$, $\Omega^2 = \frac{2\Phi_2^2 - \Phi_1^2 - \Phi_3^2}{\sqrt{6}}$, which diagonalize the AFD contribution to the free energy. Similar substitution for polarization components, $P^2 = \frac{P_1^2 + P_2^2 + P_3^2}{\sqrt{3}}$, $Q^2 = \frac{P_3^2 - P_1^2}{\sqrt{2}}$, $R^2 = \frac{2P_2^2 - P_1^2 - P_3^2}{\sqrt{6}}$, diagonalizes the FE energy. Namely:

$$\Delta G_{AFD}^{2-4}[\Phi, \Psi, \Omega] = \sqrt{3}b_1\Phi^2 + (b_{11} + b_{12})\Phi^4 + \left(b_{11} - \frac{b_{12}}{2}\right)(\Psi^4 + \Omega^4), \quad (8a)$$

$$\Delta G_{FE}^{2-4}[P, Q, R] = \sqrt{3}a_1P^2 + (a_{11} + a_{12})P^4 + \left(a_{11} - \frac{a_{12}}{2}\right)(Q^4 + R^4). \quad (8b)$$

Expressions (8) have the four global equivalent minimums in the AFD-FE phase, that is stable at $b_1 < 0$, $b_{11} - \frac{b_{12}}{2} > 0$, $a_1 < 0$, $a_{11} - \frac{a_{12}}{2} > 0$. The minimums coordinates are

$$\{\Phi, \Psi, \Omega, P, Q, R\} = \left\{ \pm \sqrt{-\frac{\sqrt{3}b_1}{2(b_{11} + b_{12})}}, 0, 0, \pm \sqrt{-\frac{\sqrt{3}a_1}{2(a_{11} + a_{12})}}, 0, 0 \right\} \quad (9)$$

in the six dimensional (6D) phase space. The minimum corresponds to the conventional R3c phase of

$$\text{BFO}, \Phi_1^2 = \Phi_2^2 = \Phi_3^2 = -\frac{b_1}{2(b_{11} + b_{12})} \text{ and } P_1^2 = P_2^2 = P_3^2 = -\frac{a_1}{2(a_{11} + a_{12})}.$$

Nonzero biquadratic coupling $\zeta_{ijkl}\Phi_i\Phi_jP_kP_l$ given by Eq.(4), as well as 6-th order powers Φ_i^6 and P_i^6 included in Eqs.(2)-(3), makes the diagonalization impossible, the minimum can be shifted, and, moreover, some of the minima can become metastable or even disappear due to the biquadratic coupling and 6-order terms contribution. Specifically, in normal coordinates the "isotropic" part of biquadratic form ΔG_{BQC}^{11} can be identically rewritten as:

$$\Delta G_{BQC}^{11} = \zeta_{11}(\Phi_1^2P_1^2 + \Phi_2^2P_2^2 + \Phi_3^2P_3^2) \equiv \zeta_{11}(\Phi^2P^2 + \Psi^2Q^2 + \Omega^2R^2) \quad (10)$$

Thus, the oversimplified free energy (7)-(8) with the isotropic coupling (10) included has the form

$$\Delta G_{AFD-FE}^{2-4} = \left[\begin{aligned} &\sqrt{3}b_1\Phi^2 + (b_{11} + b_{12})\Phi^4 + \left(b_{11} - \frac{b_{12}}{2}\right)(\Psi^4 + \Omega^4) + \sqrt{3}a_1P^2 + \\ &(a_{11} + a_{12})P^4 + \left(a_{11} - \frac{a_{12}}{2}\right)(Q^4 + R^4) + \zeta_{11}(\Phi^2P^2 + \Psi^2Q^2 + \Omega^2R^2) \end{aligned} \right] \quad (11)$$

The energy (11) also has four energetically equivalent minimums with coordinates

$$\{\Phi, \Psi, \Omega, P, Q, R\} = \left\{ \pm \sqrt{\frac{\sqrt{3}[a_1\zeta_{11} - 2b_1(a_{11} + a_{12})]}{4(b_{11} + b_{12})(a_{11} + a_{12}) - \zeta_{11}^2}}, 0, 0, \pm \sqrt{\frac{\sqrt{3}[b_1\zeta_{11} - 2a_1(b_{11} + b_{12})]}{4(a_{11} + a_{12})(b_{11} + b_{12}) - \zeta_{11}^2}}, 0, 0 \right\} \quad (12)$$

These minima correspond to R3c phase in a bulk AFD-FE multiferroic with isotropic biquadratic coupling. Unfortunately, we could not find any analytical expressions for the full anisotropic form of biquadratic coupling (4) included in the free energy.

Free energy surface cross-sections was calculated without ($\zeta_{ijkl} = 0$) and with ($\zeta_{ijkl} \neq 0$) biquadratic coupling, and the role of the ζ_{ijkl} contribution can be imagined from the comparison of **Fig.2(a)** and **Fig.2(b)**. Calculations were performed for the 2-4-6 coupled free AFD-FE energy (1)-(6) of BFO that's evident form is listed in **Appendix A** with numerical parameters from **Table I**. Four equivalent minima with coordinates similar to the ones given by Eq.(9), which are separated by a local maximum at the coordinate origin, correspond to the case $\zeta_{ijkl} = 0$ [see **Fig.2(a)**]. The small difference in minima coordinates originated from the contribution of the 6-th powers of the order parameters, which are not included in Eqs.(8)-(9). Two equivalent global minima and two shallow local minima different from the ones given by Eq.(12), which are separated by a local maximum at the coordinate origin, exist for the case $\zeta_{ijkl} \neq 0$ [see **Fig.2(b)**]. The difference originated from the terms $\sim \zeta_{12}(\Phi_1\Phi_2P_1P_2 + \dots)$ in the biquadratic coupling energy (4), rather than from the 6-th powers of the order parameters.

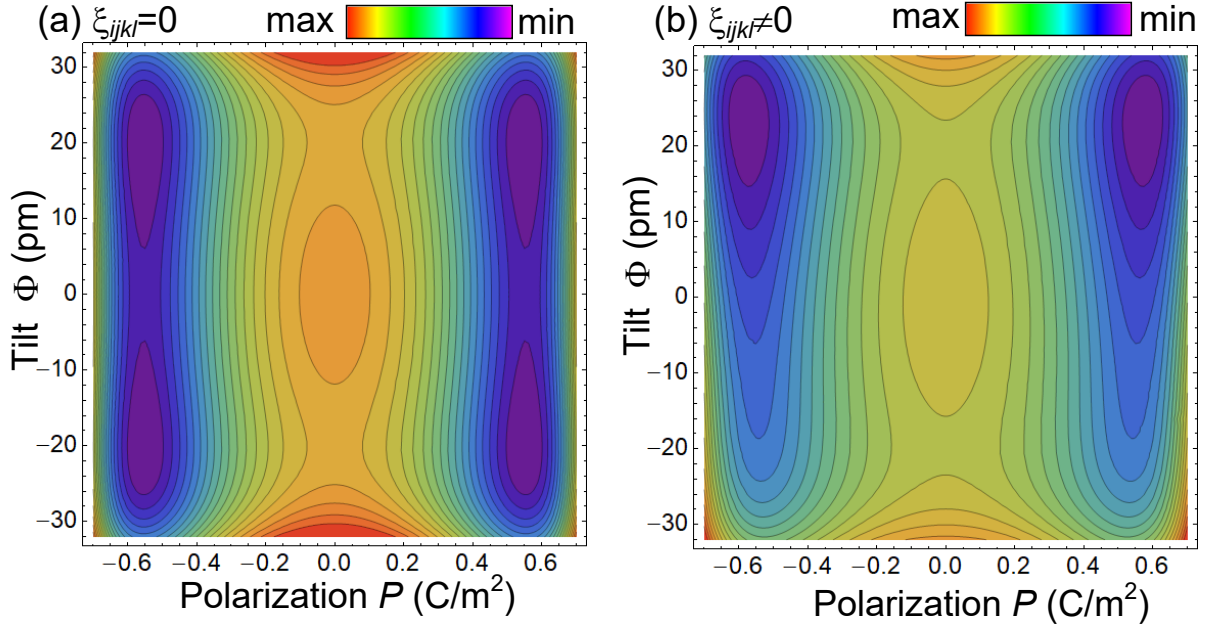


FIGURE. 2. Free energy surface cross-section in "normal" coordinates $\{\Phi, P\}$ calculated at room temperature without **(a)** and with **(b)** biquadratic coupling ζ_{ijkl} contribution. The cross-sections show the deepest minima corresponding to the case $\Psi = \Omega = Q = R = 0$. BFO parameters are listed in **Table I**.

The cross-sections shown in **Fig.2 (b)** contain the deepest minima, which correspond to nonzero coordinates $\{\Phi, P\}$ and zero coordinates $\Psi = \Omega = Q = R = 0$, i.e. $\Phi_1^2 = \Phi_2^2 = \Phi_3^2$ and $P_1^2 = P_2^2 = P_3^2$, that is a stable R3c phase. We checked numerically, that no other local (or global) minima correspond to nonzero $\{\Psi, \Omega, Q, R\}$ exist for the material parameters of realistic BFO listed in **Table I**. Hence among all homogeneous phases, only R3c phase is absolutely stable below T_C and lower temperatures in a bulk BFO without gradient energy. The result is expected and confirms the appropriate choice of the form and numerical parameters in the free energy (1)-(5). That is why any other (meta)stable phases or/and domain configurations, different from R3c, which will be revealed and analyzed in the next sections, cannot originate from the local minima in the free energy (1)-(5).

Table I. Parameters used in LGD calculations for "tilted" perovskite BFO

Parameter	Designation	Numerical value for BFO
background permittivity	ϵ_b	7
dielectric stiffness	α_T ($\times 10^5 \text{C}^{-2} \cdot \text{Jm/K}$)	9
Curie temperature for P	T_C (K)	1300
Barret temperature for P	T_{qP} (K)	800
polar expansion 4 th order	a_{ij} ($\times 10^8 \text{C}^{-4} \cdot \text{m}^5 \text{J}$)	$a_{11} = -13.5, a_{12} = 5$

LGD expansion 6 th order	a_{ijk} ($\times 10^9 \text{C}^{-6} \cdot \text{m}^9 \text{J}$)	$a_{111}=11.2, a_{112}=-3, a_{123}=-6$
electrostriction	Q_{ij} ($\text{C}^{-2} \cdot \text{m}^4$)	$Q_{11}=0.03, Q_{12}=-0.01, Q_{44}=0.01$
compliances	s_{ij} ($\times 10^{-12} \text{Pa}^{-1}$)	$s_{11}=8.3, s_{12}=-2.7, s_{44}=9.25$
Polarization gradient coefficients	g_{ij} ($\times 10^{-10} \text{C}^{-2} \text{m}^3 \text{J}$)	$g_{11}=5, g_{12}=-0.5, g_{44}=0.5$
Roto-electric coupling	$\times 10^{29} \text{C}^{-2} \cdot \text{m}^2 \text{J/K}$	$\xi_{11}=-0.5, \xi_{12}=0.5, \xi_{44}=-2.6$
Tilt expansion 2 nd order	b_T ($\times 10^{26} \text{J}/(\text{m}^5 \text{K})$)	4
Curie temperature for Φ	T_Φ (K)	1440
Barret temperature for Φ	$T_{q\Phi}$ (K)	400
Tilt expansion 4 nd order	b_{ij} ($\times 10^{48} \text{J}/(\text{m}^7)$)	$b_{11}=-24+4.5 (\coth(300/T) - \coth(3/14))$ $b_{12}=45-4.5 (\coth(300/T) - \coth(1/4))$
Tilt expansion 6 nd order	b_{ijk} ($\times 10^{70} \text{J}/(\text{m}^9)$)	$b_{111}=4.5-3.4 (\coth(400/T) - \coth(2/7))$ $b_{112}=3.6-0.04 (\coth(10/T) - \coth(1/130))$ $b_{123}=41-43.2 (\coth(1200/T) - \coth(12/11))$
Tilt gradient coefficients	v_{ij} ($\times 10^{11} \text{J}/\text{m}^3$)	$v_{11}=0.25, v_{44}=(0.25-25)$
Polarization extrapolation lengths	$\lambda_i^P \equiv g_{i3}^{(P)} / a_i^{(S)}$ (nm)	Vary from "0" to high enough values > 100 nm (for comparison)
Tilt extrapolation lengths	$\lambda_i^\Phi \equiv v_{i3}^{(\Phi)} / b_i^{(S)}$ (nm)	Vary from "0" to high enough values > 100 nm (for comparison)
Surface screening length	Λ (nm)	Vary from "0" to 0.1 nm (for comparison)

III. SIMULATION RESULTS AND DISCUSSION

A. Simulation details

We used FEM to simulate the oxygen tilt and polarization distribution in thin free-standing BFO films covered by conducting electrodes. The film thickness h varied from 5 nm to 500 nm, and the typical picture of domain morphology was observed at $h > 15$ nm, so we use the thicknesses (16 – 20) nm for illustration.

To minimize the impact of the surface, we use the so-called natural polarization and tilt boundary conditions [86] to generate plots, corresponding to zero surface energy (6), i.e. to $a_i^{(S)} = b_i^{(S)} = 0$ in the boundary conditions (7b). The natural conditions correspond to the minimal critical thickness of the film. For comparison we also performed simulations for zero polarization and tilt components at the film surfaces, $P_i \big|_{x_3=0,h} = 0$ and $\Phi_i \big|_{x_3=0,h} = 0$, which corresponds to the

maximal influence of the surface and maximal critical thickness of the film. Parameters used in the FEM calculations to generate figures are listed in **Table I**.

It appeared that curved walls arise as a result of the relaxation process of a random domain distribution, named "random seeding" (see **Fig. 3**).

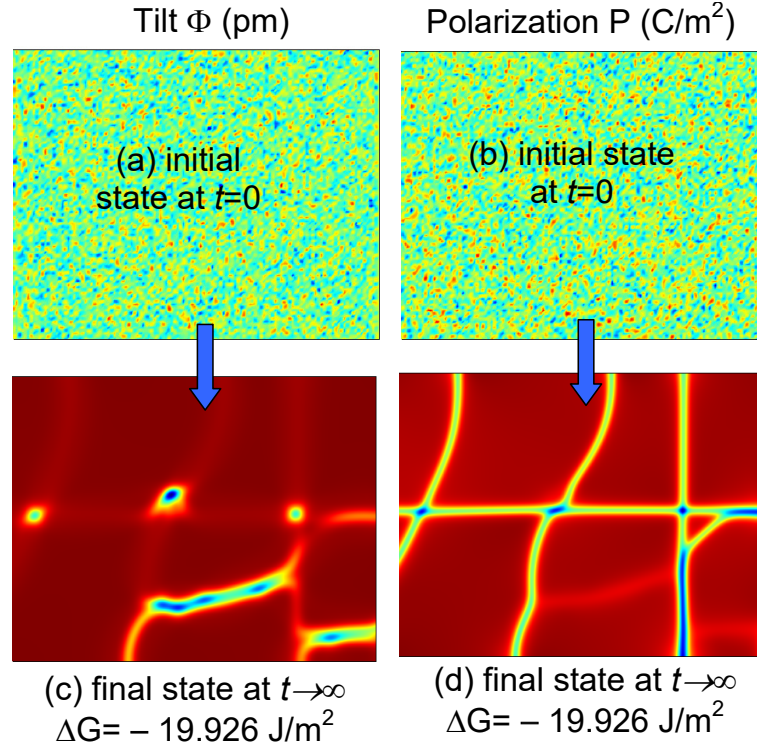


FIGURE. 3. Initial and final distributions of the tilt (**a, c**) and polarization (**b,d**) in a 16-nm BFO film at room temperature for the case of random seeding. Gradient coefficient $\nu_{44}=0.25 \times 10^{11} \text{ J/ m}^3$, $\Lambda=0$, other parameters of BFO are listed in **Table I**.

Also the random seeding can be superimposed on the ideal nominally uncharged 180-, 109- and 71-degree domain wall structure in BFO R3c phase. Initial and final domain states are shown in **Fig.4** and **Fig.S1** in **Appendix B**. From the figures the curved features appeared at the 180- and 109-degree AFD walls, but not at the 71-walls. The energy density excess ΔG corresponding to the relaxation of the initial random domain (**RD**) distribution, poly-domain distribution (**PD**) with straight 180, 109- and 71-degree domain walls; and poly-domain distribution disturbed by a random seeding (**PD + RD**) have been compared. It appeared that the energies are surprisingly close, namely $\Delta G = -19.926 \text{ J/m}^2$ for the curved domain walls obtained from the relaxation of RD (see **Fig. 3**), $\Delta G = -19.853 \text{ J/m}^2$ for the 180-degree domain walls obtained from the relaxation of PD+RD [see **Fig. 4(a)-(d)**], and $\Delta G = -19.865 \text{ J/m}^2$ for the 180-degree domain walls obtained from the relaxation

of PD [see **Fig. 4(e)-(f)**]. The proximity of the energies is a convincing argument for a long-living metastability of the curved domain walls in BFO.

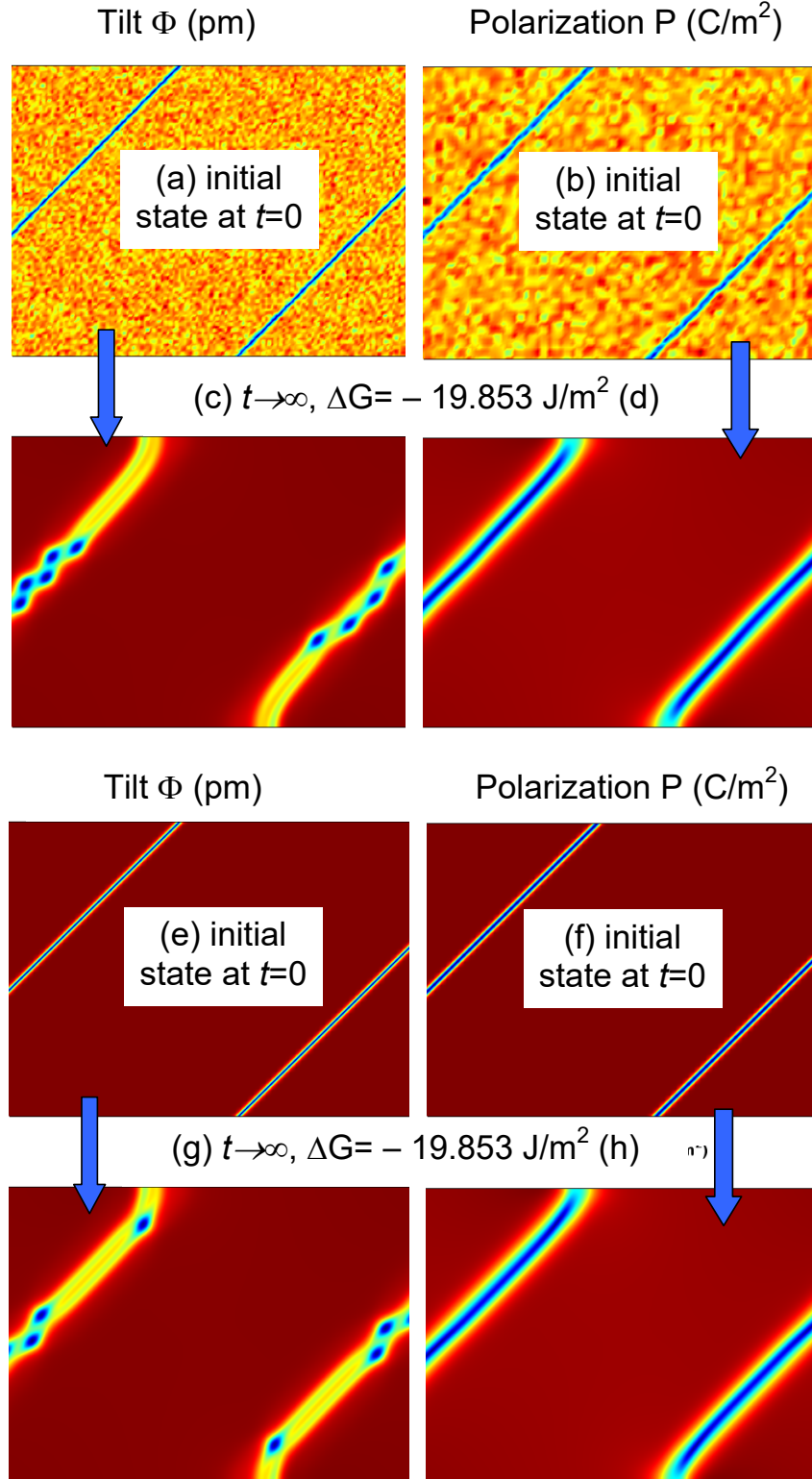


FIGURE. 4. Initial and final distributions of the tilt (**a, c**) and polarization (**b,d**) in a 16-nm BFO film at room temperature for the 180-degree domains random seeding. Gradient coefficient $\nu_{44}=0.25 \times 10^{11}$ J/ m³, $\Lambda=0$, other parameters of BFO are listed in **Table I**.

From the previous **section II.C**, we are convinced that the origin of the low symmetry AFD-FE phases is not the instability of the free energy relief with respect to the existence of local minima. So, what is the physical origin of the appearance of low symmetry phases limited by zig-zag like meandering domains at 180-degree and 109-degree domain boundaries? Why they do not exist for at 71-degree domain walls? To establish the origin, we performed the following numerical experiments.

(a) The AFD-FE domain structure (including the low symmetry domains) exists and becomes insensitive to the screening length values at $\Lambda \ll 0.1$ nm. We observed the stable low symmetry domains in the limiting case $\Lambda \rightarrow 0$ corresponding to perfect screening and minimal depolarization electric field. Hence the origin of the low symmetry phases limited by meandering antiferrodistortive-ferroelectric domain walls is not the incomplete screening of ferroelectric polarization by the imperfect electrodes or surface charge.

(b) We explored whether the low symmetry domains originate from the spatial confinement of polarization components at the film surfaces. Namely we compared the changes of the AFD-FE

domain morphology when the ratio $\lambda_i^P \equiv \frac{g_{i3}^{(P)}}{a_i^{(S)}}$ varies from 0 (corresponding to zero polarization at the film surfaces, $P_i|_{x_3=0,h} = 0$) to the opposite case $\lambda_i^P \rightarrow \infty$ (corresponding to $a_i^{(S)} = 0$ and

$\left. \frac{\partial P_i}{\partial x_3} \right|_{x_3=0,h} = 0$). For $\lambda_i^P = 0$ we see the appearance of FE domain wall broadening at the surface and it gradual decrease with increase of the ratio λ_i^P , as anticipated. However no significant changes of the low-symmetry phases limited by meandering walls in the film occur when λ_i^P changes.

(c) We further compared the changes of the AFD-FE domain structure when the ratio $\lambda_i^\Phi \equiv \frac{v_{i3}^{(\Phi)}}{b_i^{(S)}}$ varies from 0 (corresponding to zero polarization at the film surfaces, $\Phi_i|_{x_3=0,h} = 0$) to the opposite

case $\lambda_i^\Phi \rightarrow \infty$ (corresponding to $b_i^{(S)} = 0$ and $\left. \frac{\partial \Phi_i}{\partial x_3} \right|_{x_3=0,h} = 0$). For $\lambda_i^\Phi = 0$ we see the appearance of

AFD domain wall broadening at the surface and it gradual decrease with increase of the ratio λ_i^Φ , as anticipated. However, no significant changes of the domain morphology occur when λ_i^Φ changes. Further we can assume that the spatial confinement delineates the appropriate boundary conditions for the oxygen tilt and polarization components at the film surfaces.

(d) We rotate the film surface cut to find the angle for which both AFD and FE walls are straight without inclusion of any low symmetry domain phases. We made sure that the angle does not exist. Also, we checked whether the low symmetry meandering zig-zag domains originate from the spatial confinement effect delineated by the appropriate boundary conditions for the oxygen tilt at the film surfaces. We increase the film thickness h up to 500 nm and see that no significant changes in the morphology of meandering domains occur.

(e) Finally, we varied the components of the electrostrictive or flexoelectric couplings tensors in a typical range ($0 \leq |F_{ijkl}| \leq 10^{11} \text{ m}^3/\text{C}$, $0 \leq |Q_{ijkl}| \leq 0.1 \text{ m}^4/\text{C}^2$) and lead to the conclusion that the appearance of low symmetry phase does not steam from the couplings, because the low-symmetry domain structure weakly react on the changes of F_{ijkl} and Q_{ijkl} values.

(f) It appeared that the changes of the tilt gradient coefficients $v_{ijkl}^{(\Phi)}$ significantly affects on the domain structure including the monoclinic phase appearance. The impact of the polarization gradient coefficients $g_{ijkl}^{(P)}$, is much less pronounced, because the polarization FE walls do not bend in order to remain uncharged. The charging of FE wall by the polarization bound charge will immediately lead to the appearance of strong depolarization electric field E_i^d ($\text{div} \vec{E}^d \sim -\text{div} \vec{P}$) that's energy excess $-E_i^d P_i/2$ is positive at the region of curved wall and relatively high. Thus, the polar sub-system behaves in such a way to prevent the charging.

From the analyses of (a)-(f) we concluded that the origin of the low symmetry AFD-FE domains is due to the coupling between the tilts and polarization gradient coefficients. This conclusion is consistent with the results of Conti et al. [87], who used a simple phenomenological model and have shown that for multiferroics with symmetric free energy and two order parameters, in the mixed phase (i.e., when both order parameters are nonzero), a maximum and minimum near the antiphase domain walls appear on the profile of one of the order parameters depending on the anisotropy gradient energy. Despite the fact that we considered a much more complex system with six order parameters, the extremums observed near the domain walls are qualitatively similar to the phenomenon predicted by Conti et al. Thus, the appearance of maxima and minima on the profiles of the order parameters near the domain walls can be associated with the features (such as anisotropy) of the gradient energy.

To quantify the statement, **Table II** lists analytical expressions and numerical values of correlation lengths L_C determining the domain wall width in BFO. It is seen that L_C varies significantly at the 180-degree domain wall for the different tilts (from 3.72 Å for Φ_1 to 0.78 Å Φ_3) and polarization (from 6.20 Å for P_1 to 2.38 Å to P_2) components. Tilts and polarization changes at

109-degree domain wall behave as in the hypothetic "isotropic" ferroic, namely $L_C = 1.75 \text{ \AA}$ for both tilt components and $L_C = L_C = 1.75 \text{ \AA}$ for both polarizations. Contrary, only the components Φ_3 and P_3 varies across the 71-degree domain wall, at that $L_C = 1.75 \text{ \AA}$ for Φ_3 and $L_C = 2.38 \text{ \AA}$ for P_3 .

Table II. Order parameter correlation lengths L_C determining the domain wall width in BFO

Order parameter	Type of the uncharged domain wall		
	180 degree	109 degree	71 degree
Φ_1	$L_C = \sqrt{\frac{v_{11} + v_{12} + 2v_{44}}{-4b_1}} = 3.72 \text{ \AA}$	Non applicable, since $\Phi_1 \approx \text{const}$	Non applicable, since $\Phi_1 \approx \text{const}$
Φ_2	$L_C = \sqrt{\frac{v_{44}}{-2b_1}} = 1.75 \text{ \AA}$	$L_C = \sqrt{\frac{v_{44}}{-2b_1}} = 1.75 \text{ \AA}$	Non applicable, since $\Phi_2 \approx \text{const}$
Φ_3	$L_C = \sqrt{\frac{v_{11} - v_{12}}{-4b_1}} = 0.78 \text{ \AA}$	$L_C = \sqrt{\frac{v_{44}}{-2b_1}} = 1.75 \text{ \AA}$	$L_C = \sqrt{\frac{v_{44}}{-2b_1}} = 1.75 \text{ \AA}$
P_1	$L_C = \sqrt{\frac{g_{11} + g_{12} + 2g_{44}}{-4a_1}} = 6.20 \text{ \AA}$	Non applicable, since $P_1 \approx \text{const}$	Non applicable, since $P_1 \approx \text{const}$
P_2	$L_C = \sqrt{\frac{g_{44}}{-2a_1}} = 2.38 \text{ \AA}$	$L_C = \sqrt{\frac{g_{44}}{-2a_1}} = 2.38 \text{ \AA}$	Non applicable, since $P_2 \approx \text{const}$
P_3	$L_C = \sqrt{\frac{g_{11} - g_{12}}{-4a_1}} = 4.87 \text{ \AA}$	$L_C = \sqrt{\frac{g_{44}}{-2a_1}} = 2.38 \text{ \AA}$	$L_C = \sqrt{\frac{g_{44}}{-2a_1}} = 2.38 \text{ \AA}$

B. Low symmetry phases limited by 180-degree meandering zig-zag AFD-FE domains

Using FEM of the AFD and FE properties of strain-free thin BFO films, we further observe that the conventional 180°-domains of bulk rhombohedral AFD-FE phase [see **Fig.1(a)**] are separated by the "zig-zag" like meandering domain walls, which in fact contains thin AFD-FE domains of lower symmetry [see **Fig. 5**].

These features of the "secondary" domain structure with "zig-zag" meandering are in fact boundaries separating monoclinic domains of different parity. In this case, the domain contrast, determined by the magnitude of the tilt vector components Φ_i , is higher in the vicinity of the meandering wall in comparison with the contrast in the centre of the domain [see dark-red and dark-

blue regions near domain boundaries in **Fig. 5(a)-(c)**]. Surprisingly, neither curvature nor enhanced contrast is inherent to the ferroelectric component of the 180-degree domain boundaries [see straight incline domain boundaries with gradually changing color from red to blue in **Fig. 5(d)-(f)**]. Actually, the contrast enhancement in the zig-zag meandering regions [marked by the ellipse in **Fig. 5(b)**] does not correspond to the bulk rhombohedral phase and represents itself the region of low symmetry domains with $\Phi_1 \neq \Phi_2 \neq \Phi_3$ imposed on the 180-degree AFD-FE domains in the rhombohedral phase.

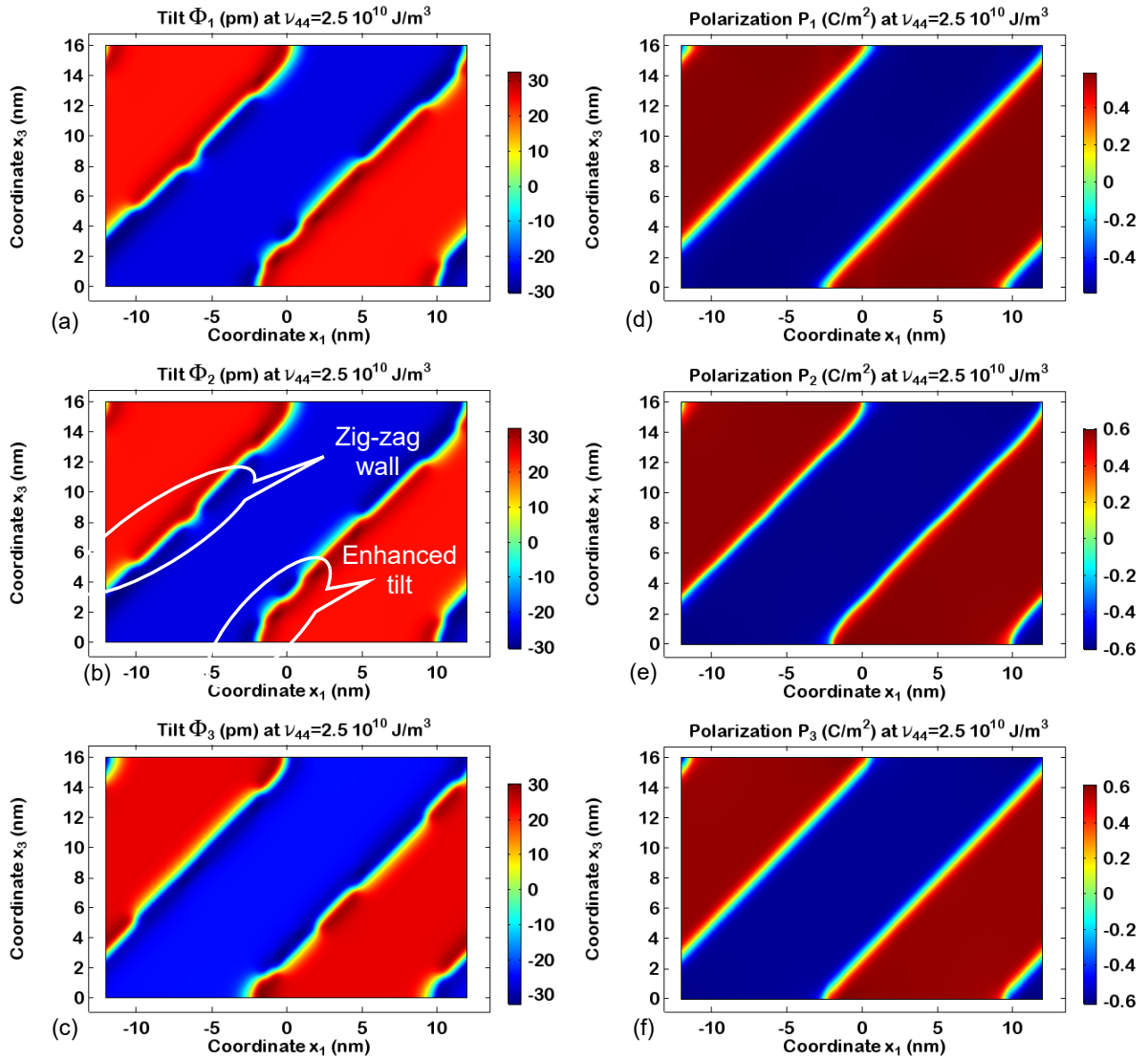


FIGURE 5. Distribution of different components of the AFD order parameter Φ_i (a)-(c) and polarization P_i (d)-(f) in a thin BFO film at room temperature. AFD-FE 180-degree domains of R3c phase are separated by zig-zag meandering domains, which in fact contain thin domains of low (monoclinic) symmetry phase. Gradient coefficient $\nu_{44}=0.25 \times 10^{11}$ J/m³, $\Lambda=0$, other parameters of BFO are listed in **Table I**.

The influence on tilt gradient coefficient value on the domain structure could be seen from **Figs. 6-7**. Meandering AFD domain walls broaden significantly and decrease their curvature with an increase of $\nu_{44}^{(\Phi)}$ by a factor of 10. In addition to significant broadening, a visible asymmetry of the wall profile appears with an increase of $\nu_{44}^{(\Phi)}$ by a factor of 100. As one could see from the figures, the amplitude of the tilt maximal deviation from bulk value is independent on gradient coefficient ν_{44} , while polarization profiles are almost independent on this parameter. Thus, we conclude that the appearance of the phases is conditioned by the decrease of the tilts gradient energy. If $\nu_{44}^{(\Phi)}$ is sufficiently small, the energy increase associated with the AFD wall bending is less than the energy decrease associated with the terms proportional to $b_{ij}\Phi_i^2\Phi_j^2$.

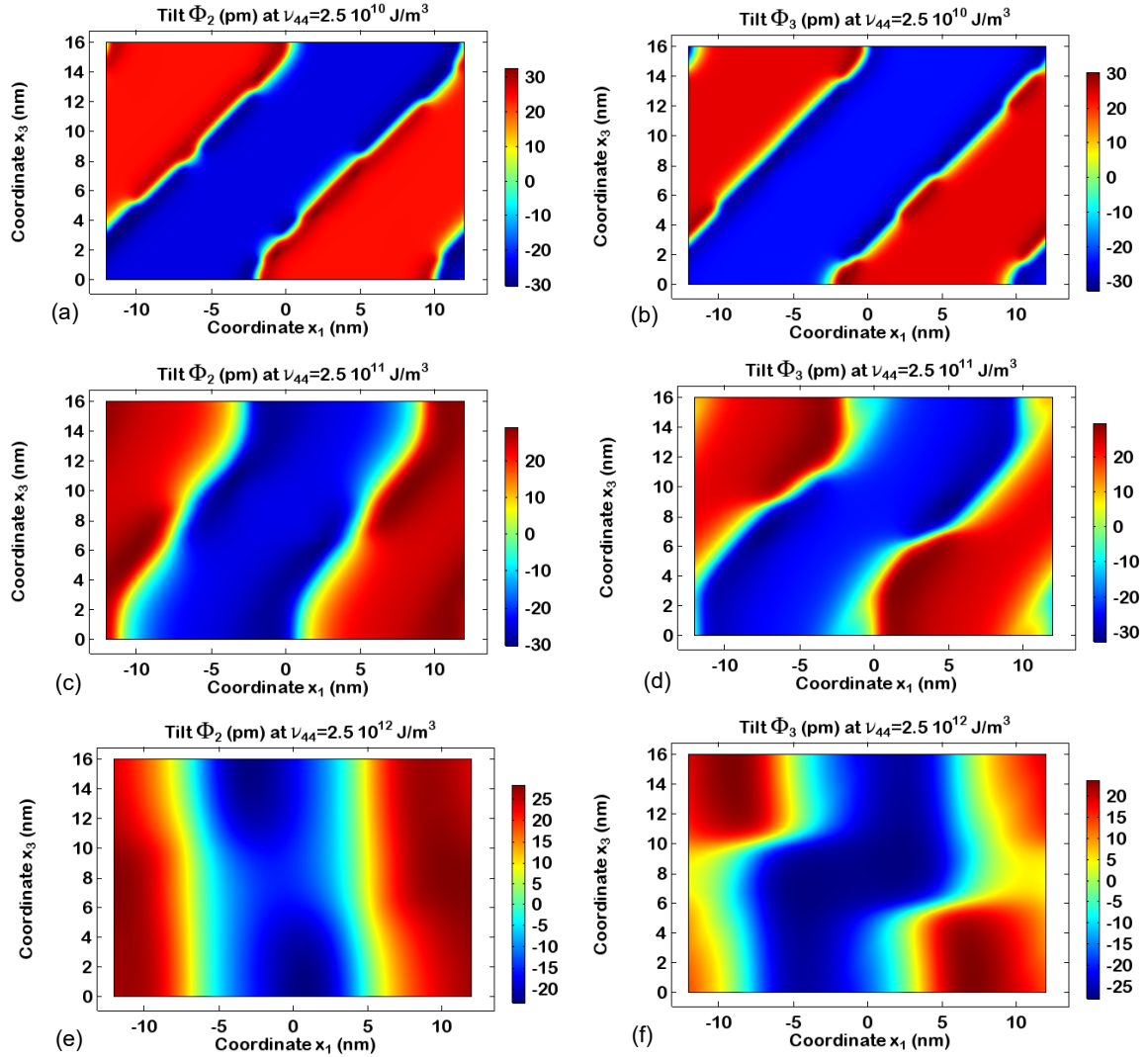


FIGURE 6. Distribution of different components of the AFD order parameter Φ_2 (**a, c, e**) and Φ_3 (**b, d, f**) in a thin BFO film at room temperature for different values of gradient coefficient $\nu_{44}=0.25$ (**a, b**), 2.5 (**c, d**), and 25 (**e, f**) (in units of 10^{11} J/m³); $\Lambda=0$, other parameters of BFO are listed in **Table I**.

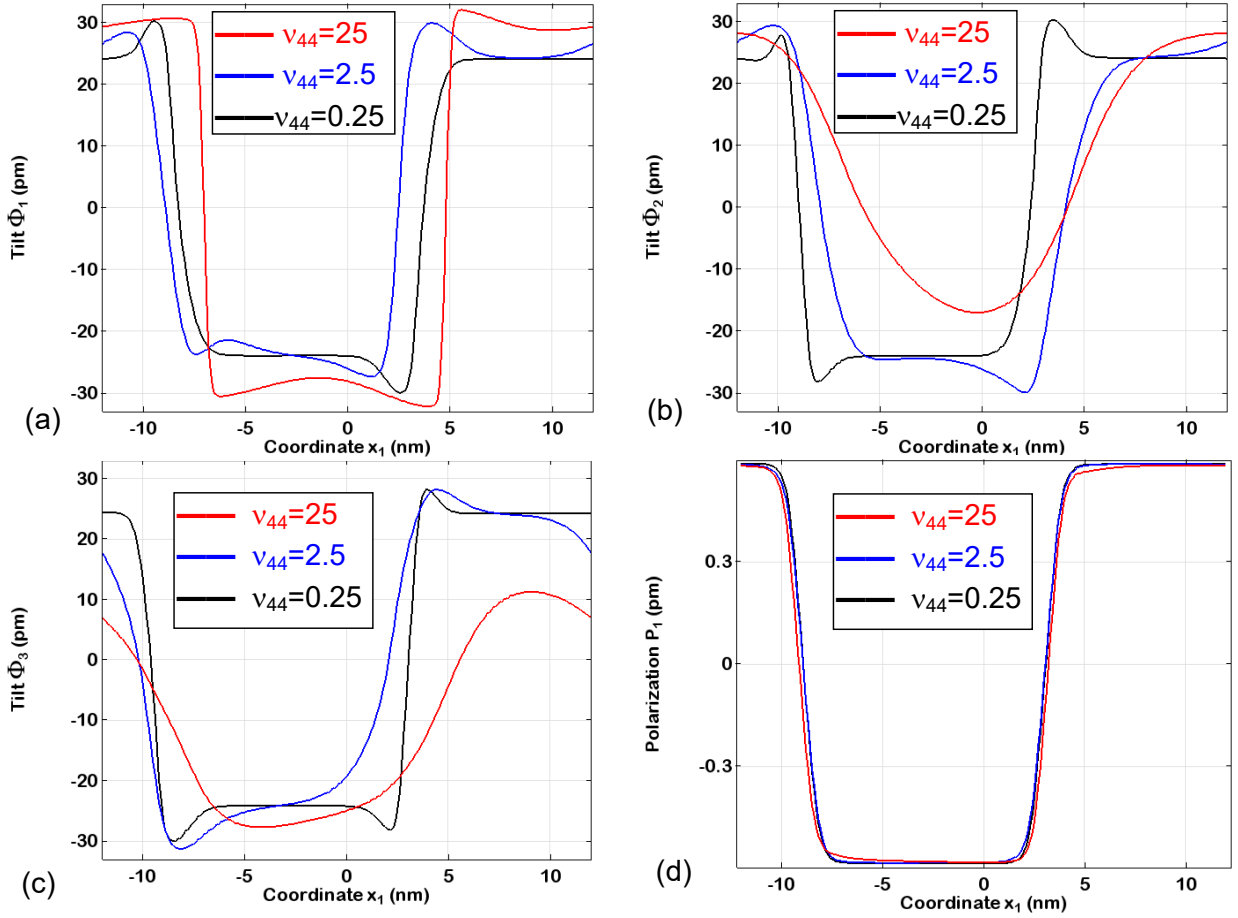


FIGURE 7. Distribution of different components of the AFD order parameter Φ_i (a, b, c), and polarization P_2 (d) calculated in the middle of thin BFO film ($x_3 = h/2$) at room temperature for different values of gradient coefficient $v_{44}=0.25$ (black), 2.5 (blue) and 25 (red) in units of 10^{11} J/m³; $\Lambda=0$, other parameters of BFO are listed in **Table I**.

C. Low symmetry phases limited by 109-degree zig-zag meandering AFD-FE domains

Bulk 109-degree domains correspond to the case when two components of vectorial order parameter changes its sign when crossing the wall plane [see **Fig. 1(b)**]. These are Φ_2 , Φ_3 and P_2 , P_3 respectively for the tilt and polarization as the two vectorial order parameters. These domains of bulk rhombohedral phase are separated by the AFD "zig-zig" domain walls, which in fact contains thin domains of low symmetry phase [see **Figs. 8**]. Enhanced contrast is also inherent to the ferroelectric component of the domain boundaries [see domain boundaries with gradually changing color from red to blue in **Figs. 8(a)-(c)**]. Actually, the contrast enhancement in the zig-zag meandering regions do

not correspond to the bulk rhombohedral R3c phase and are the region of low symmetry domains with $\Phi_1 \neq \Phi_2 \neq \Phi_3$ and $P_1 \neq P_2 \neq P_3$ imposed on the twin boundaries in the rhombohedral bulk.

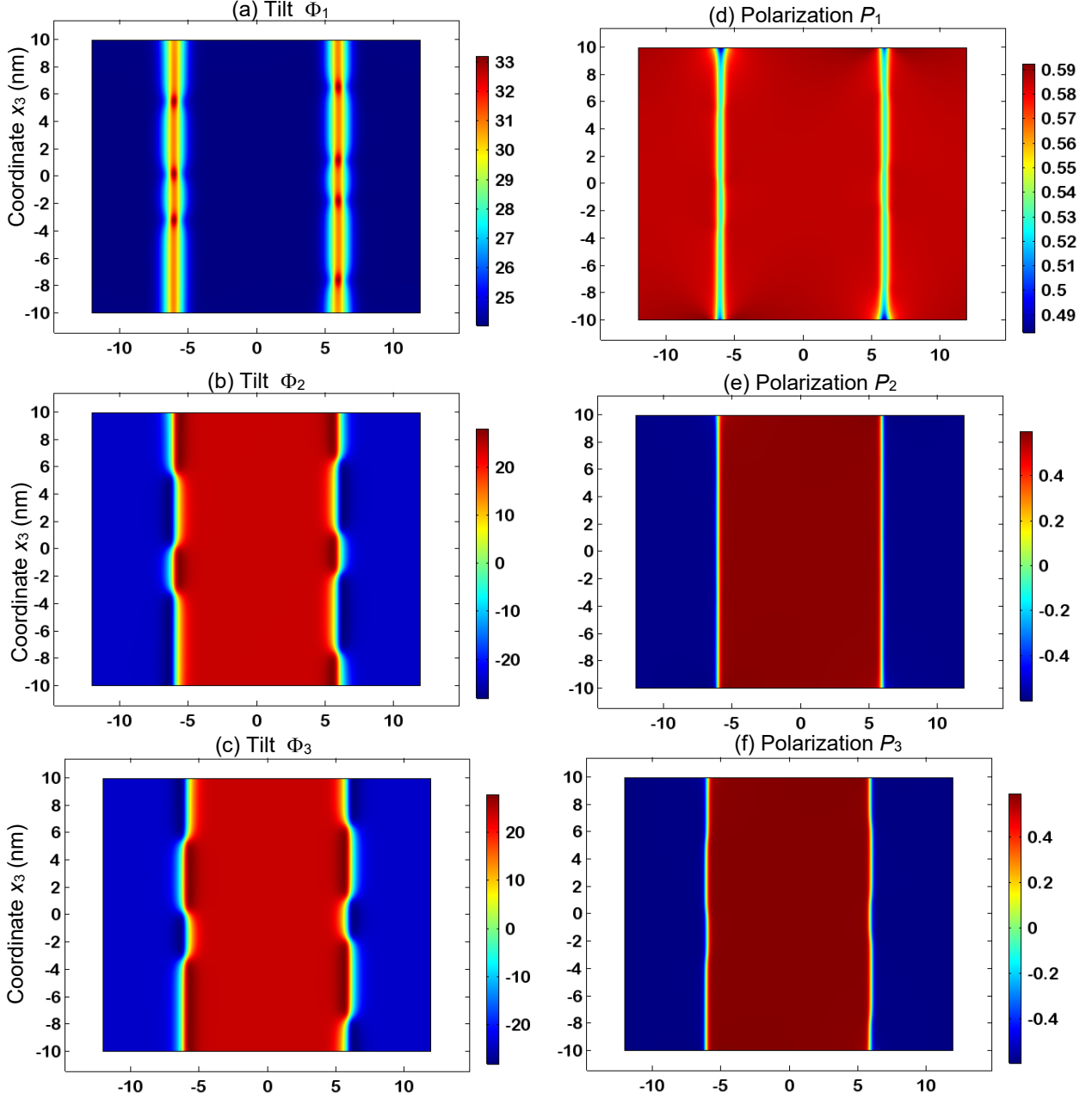


FIGURE 8. Distribution of different components of the AFD order parameter Φ_i (a)-(c) and polarization P_i (d)-(f) in a thin BFO film at room temperature. AFD 109-degree domains of R3c phase are separated by zig-zag like meanders, which in fact contains thin domains of low symmetry phase. LGD parameters are listed in Table I, Appendix A.

Similarly to the case of the low symmetry AFD-FE phases appearing the vicinity of 180-degree domain walls (considered in section III.B) we made sure that the appearance of unusual low

symmetry domains at 109-degree domain walls does not stem from the spatial confinement or imperfect screening of spontaneous polarization, electrostrictive or flexoelectric couplings, but rather from the interplay between the gradient of the oxygen tilt and polarization components at the domain walls. Indeed, the influence on the tilt gradient coefficient value is shown in **Fig. 9**. Distributions of order parameters in the cross sections in the middle of the film, corresponding to **Fig. 9**, are shown in **Fig. 10**.

One could see two tendencies with increase of v_{44} . The first tendency is an obvious increase of domain wall width (proportionally to $v_{44}^{1/2}$) and the second one is the decrease of the “secondary walls” density and curvature, which separate low symmetry domains. As one could see from **Fig. 10**, the amplitude of the tilt maximal deviation from a bulk value is independent on gradient coefficient v_{44} . However the low symmetry phases over-occupy the central part of BFO film for the high values of v_{44} . For the case this phase is characterized by the different amplitudes of the tilt components even far from the 109-degree domain walls.

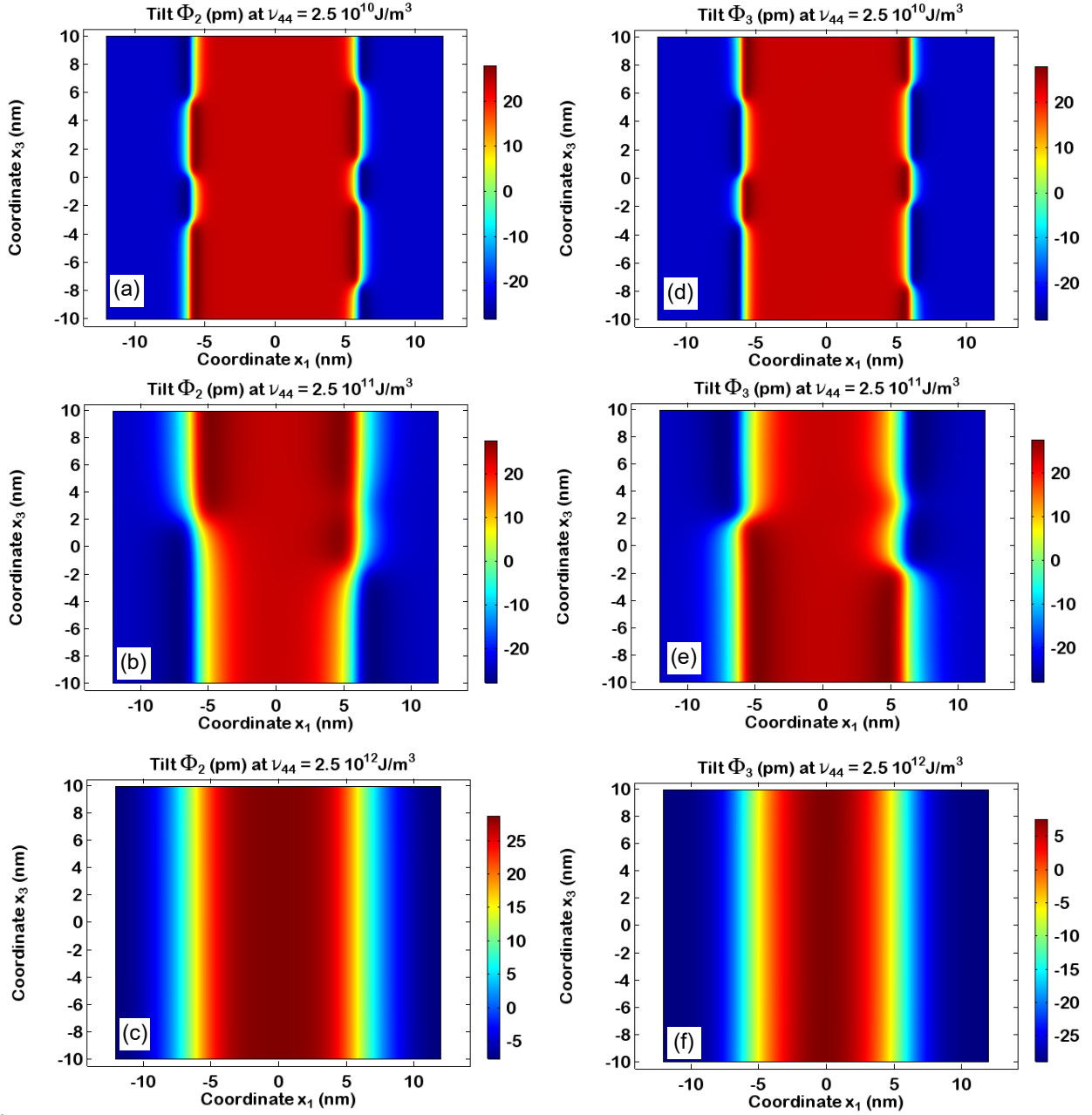


FIGURE 9. Distribution of different components of the AFD order parameter Φ_2 (a)-(d) and Φ_3 (e)-(h) in a thin BFO film at room temperature for the case of 109° -domains and different values of gradient coefficient $\nu_{44}=0.25$ (a, e), 0.5 (b, f), 1 (c, g) and 2 (d, h) (in units of 10^{11} J/m^3); other LGD parameters are listed in Table I in Appendix A.

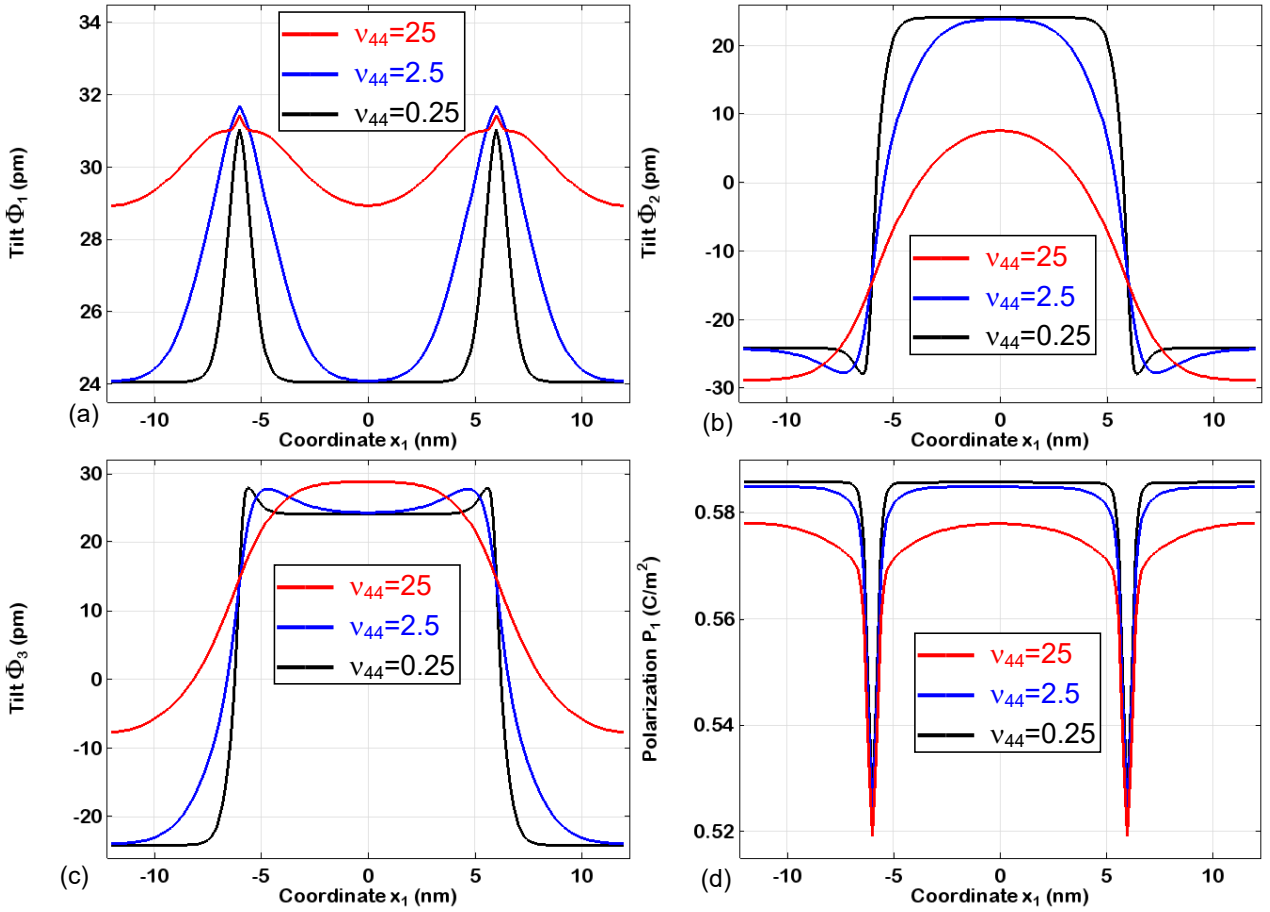


FIGURE 10. Distribution of different components of the AFD order parameter Φ_2 (a, b, c), and polarization P_2 (d) calculated for the case of 109° -domains in the middle of thin BFO film ($x_3 = h/2$) at room temperature for different values of gradient coefficient $v_{44}=0.25$ (black), 2.5 (blue) and 25 (red) in units of 10^{11} J/m^3 ; other LGD parameters are listed in **Table I** in **Appendix A**.

D. Antiferrodistortive-ferroelectric 71-degree domain walls. Domain wall broadening

Bulk 71-degree domains correspond to the case when only one component of vectorial order parameter changes its sign when crossing the wall plane [see **Fig.1(c)**]. It is Φ_2 and P_2 in the considered case of rhombohedral phase of BFO. The results of calculations are presented in **Figs. 11-12**.

Slight bending of the domain wall at the surface is determined by internal electric field, especially due to the appearance of out-of-plane component near the surface (see **Fig. S.2b**). The in-plane component of field is maximal at the domain walls far from the surface (see **Fig. S.2a**). This effect is caused by the variation of in-plane component of polarization P_1 (see **Figs. 11d**) perpendicular to the wall due to the coupling with other components of polarization and tilt. However, at the surface the electric field should be perpendicular to it, hence component E_1 tends to

zero here (see **Fig. S.2a**) and the junction surface/domain wall acts as a source of stray electric field, causing to wall bending and broadening in this region.

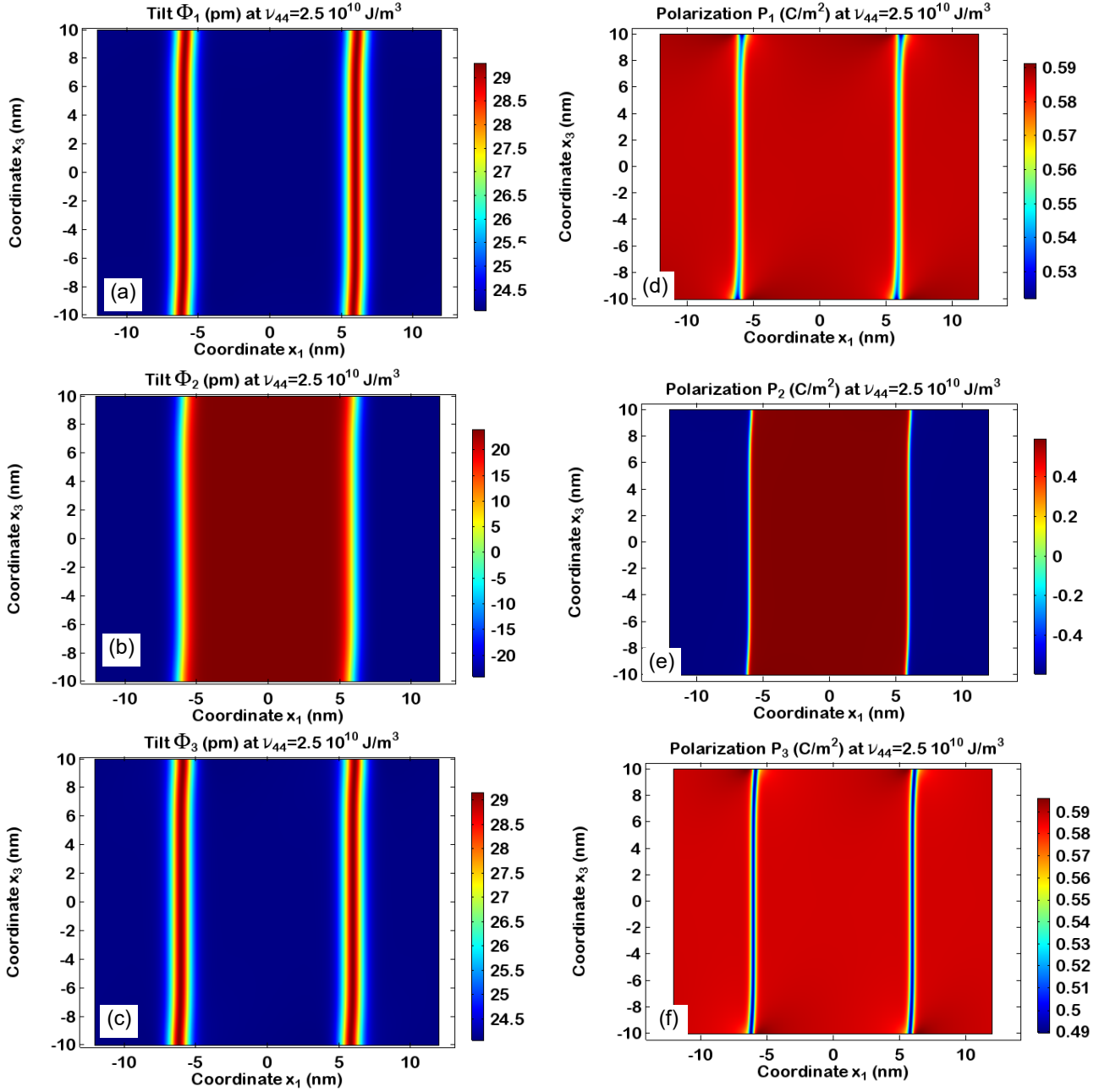


FIGURE 11. Distribution of different components of the AFD order parameter Φ_i (a)-(c) and polarization P_i (d)-(f) in a thin BFO film at room temperature for the case of 71°-domains with [100] walls. Gradient coefficient $\nu_{44} = 0.25 \times 10^{11} \text{ J/m}^3$, other LGD parameters are listed in **Table I**.

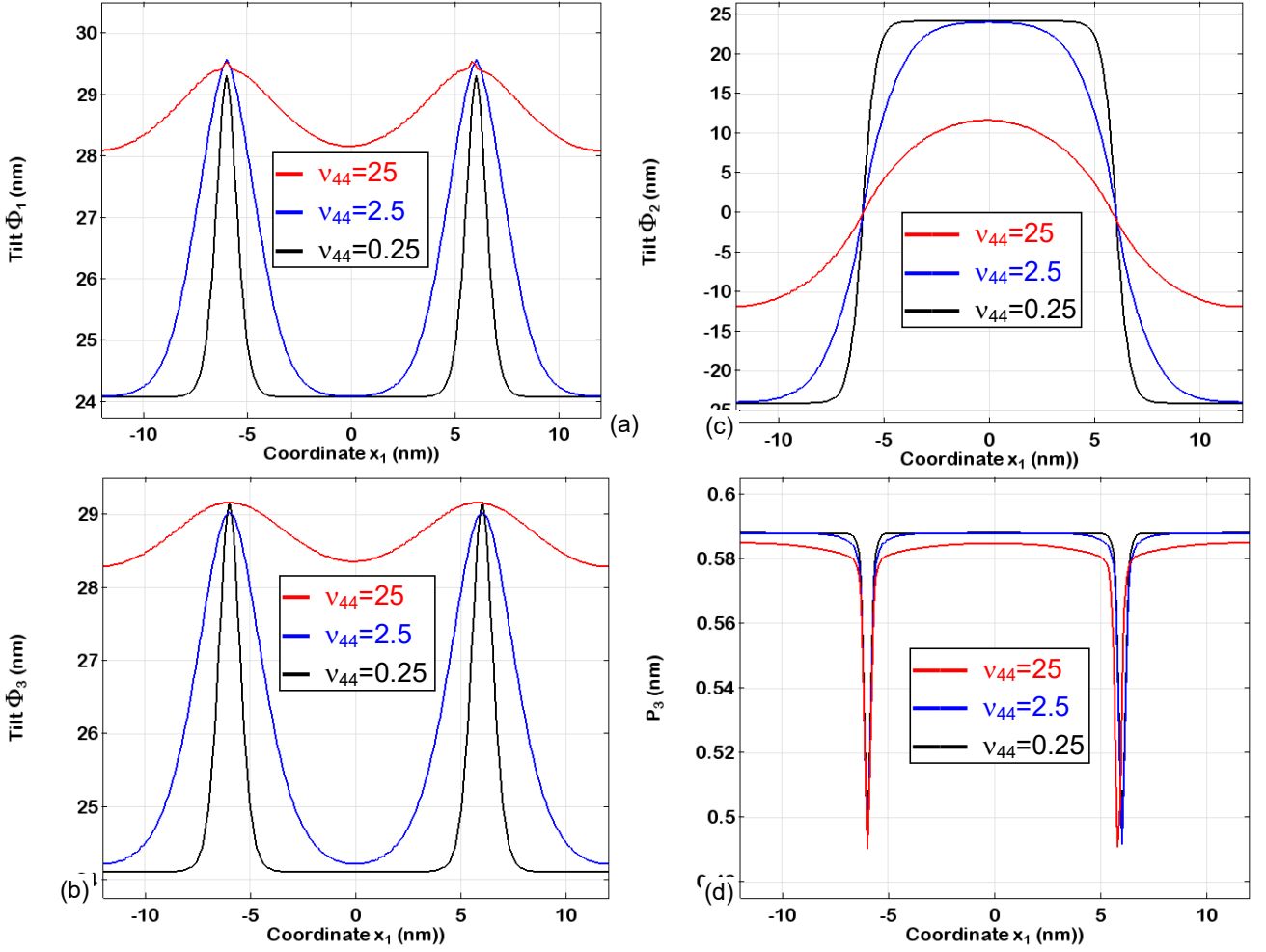


FIGURE 12. Distribution of different components of the AFD order parameter Φ_1 (a), Φ_3 (b), Φ_2 (c), and polarization component P_3 (d) at the surface of thin BFO film at room temperature for the case of 71° -domains and different values of gradient coefficient $v_{44}=0.25, 2.5$ and 25 (in units of 10^{11} J/ m³), see legends; other LGD parameters are listed in **Table I**.

IV. CONCLUSIONS

Using LGD-approach we reveal unusual low symmetry phases limited by meandering zig-zag like AFD-FE domain walls in BFO. It appeared that the origin of the low symmetry AFD-FE phases is not the instability of the free energy relief with respect to the appearance of local minima. On the contrary the appearance of the phases is conditioned by the decrease of the tilts gradient energy.

Moreover, the origin of the meandering walls does not steam from incomplete polarization screening in thin BFO films, electrostrictive or flexoelectric coupling. The spatial confinement delineates the appropriate boundary conditions for the oxygen tilt and polarization components at the film surfaces, but its existence is not critical for the meandering walls appearance and their zig-zag stability. The values of the gradient energy for the oxygen tilt appeared critical to initiate the

morphological changes of the 180– and 109 –degree uncharged domain walls towards zig-zag meandering. Zig-zag instability appears for small gradient energies, while the walls become straight and broaden at higher gradients. Uncharged 71-degree walls are always straight and their width increase with the tilt gradient coefficient increase.

Hence we predicted previously unexplored type of the gradient-driven morphological phase transition taking place at the AFD-FE domain walls in multiferroics.

Acknowledgements

A.N.M work has received funding from the European Union’s Horizon 2020 research and innovation programme under the Marie Skłodowska-Curie grant agreement No 778070, and partially supported by the National Academy of Sciences of Ukraine (project No. 0117U002612). S.V.K. and C.T.N. was supported by the Center for Nanophase Materials Sciences, sponsored by the Division of User Facilities, Basic Energy Sciences, US Department of Energy.

Authors' contribution. E.A.E. wrote the codes, performed numerical calculations and prepared figures. A.N.M. generated research idea, stated the problem, derived analytical results and wrote the manuscript draft. E.A.E. and A.N.M. contributed equality to the results interpretation. C.T.N. and S.V.K. worked on the results discussion and manuscript improvement.

REFERENCES

-
- [1] V. Wadhawan, *Introduction to Ferroic Materials*, CRC Press (2000).
 - [2] M. Fiebig, Revival of the magnetoelectric effect, *Journal of Physics D: Applied Physics* 38, R (2005).
 - [3] N. A. Spaldin and M. Fiebig, The renaissance of magnetoelectric multiferroics, *Science* 309, 391 (2005).
 - [4] J.M. Rondinelli and N.A. Spaldin, Structure and properties of functional oxide thin films: insights from electronic-structure calculations, *Advanced materials* 23, 3363 (2011).
 - [5] A. P. Pyatakov and A. K.Zvezdin, Magnetoelectric and multiferroic media, *Physics-Uspekhi* 55, 557 (2012).
 - [6] J. F. Scott, Data storage: Multiferroic memories, *Nature materials* 6, 256 (2007).
 - [7] M. Fiebig, T. Lottermoser, D. Meier, and M. Trassin, The evolution of multiferroics, *Nature Reviews Materials* 1, 16046 (2016)
 - [8] E.V. Balashova and A.K. Tagantsev, Polarization response of crystals with structural and ferroelectric instabilities, *Phys. Rev. B* 48, 9979 (1993).
 - [9] G. Catalan and James F. Scott, Physics and applications of bismuth ferrite, *Adv. Mater.* 21, 2463 (2009).
 - [10] V. Gopalan and D.B. Litvin, Rotation-reversal symmetries in crystals and handed structures, *Nature Materials* 10, 376 (2011).

-
- [11] M. J. Haun, E. Furman, T. R. Halemane, and L. E. Cross, Thermodynamic theory of the lead zirconate-titanate solid solution system, part IV: Tilting of the oxygen octahedra, *Ferroelectrics*, **99**, 55 (1989).
- [12] B. Houchmanzadeh, J. Lajzerowicz, and E Salje, Order parameter coupling and chirality of domain walls, *J. Phys.: Condens. Matter* **3**, 5163 (1991)
- [13] A.K. Tagantsev, E. Courtens and L. Arzel, Prediction of a low-temperature ferroelectric instability in antiphase domain boundaries of strontium titanate, *Phys. Rev. B*, **64**, 224107 (2001).
- [14] A.N. Morozovska, E.A. Eliseev, M.D. Glinchuk, L.-Q. Chen, V. Gopalan. Interfacial polarization and pyroelectricity in antiferrodistortive structures induced by a flexoelectric effect and rotostriction. *Phys. Rev. B*. **85**, 094107 (2012).
- [15] M. Daraktchiev, G. Catalan, J. F. Scott. Landau theory of domain wall magnetoelectricity. *Phys. Rev. B* **81**, 224118 (2010).
- [16] A.K. Tagantsev, L. E. Cross, and J. Fousek. *Domains in ferroic crystals and thin films*. New York: Springer, 2010. ISBN 978-1-4419-1416-3, e-ISBN 978-1-4419-1417-0, DOI 10.1007/978-1-4419-1417-0
- [17] Albina Y. Borisevich, E. A. Eliseev, A. N. Morozovska, C-J. Cheng, J-Y. Lin, Ying-Hao Chu, Daisuke Kan, Ichiro Takeuchi, V. Nagarajan, and Sergei V. Kalinin. "Atomic-scale evolution of modulated phases at the ferroelectric–antiferroelectric morphotropic phase boundary controlled by flexoelectric interaction." *Nature communications* **3**: 775 (2012).
- [18] A. K. Tagantsev, K. Vaideeswaran, S. B. Vakhrushev, A. V. Filimonov, R. G. Burkovsky, A. Shaganov, D. Andronikova, A. I. Rudskoy, A. Q. R. Baron, H. Uchiyama, D. Chernyshov, A. Bosak, Z. Ujma, K. Roleder, A. Majchrowski, J.-H. Ko & N. Setter. "The origin of antiferroelectricity in PbZrO₃." *Nature communications* **4**, article number **2229** (2013).
- [19] P. Henning, and E. KH Salje. "Flexoelectricity, incommensurate phases and the Lifshitz point". *J. Phys.: Condens. Matter* **28**, 075902 (2016).
- [20] R. G. Burkovsky, A. K. Tagantsev, K. Vaideeswaran, N. Setter, S. B. Vakhrushev, A. V. Filimonov, A. Shaganov, D. Andronikova, A.I. Rudskoy, A.Q.R. Baron, and H. Uchiyama, "Lattice dynamics and antiferroelectricity in PbZrO₃ tested by x-ray and Brillouin light scattering." *Physical Review* **B 90**, 144301 (2014).
- [21] Eugene A. Eliseev, Sergei V. Kalinin, Yijia Gu, Maya D. Glinchuk, Victoria Khist, Albina Borisevich, Venkatraman Gopalan, Long-Qing Chen, and Anna N. Morozovska. Universal emergence of spatially-modulated structures induced by flexo-antiferrodistortive coupling in multiferroics. *Phys.Rev.* **B 88**, 224105 (2013)
- [22] V. Goian, S. Kamba, O. Pacheroova, J. Drahokoupil, L. Palatinus, M. Dusek, J. Rohlíček, M. Savinov, F. Laufek, W. Schranz, A. Fuith, M. Kachlik, K. Maca, A. Shkabko, L. Sagarna, A. Weidenkaff, and A. A. Belik. Antiferrodistortive phase transition in EuTiO₃. *Phys. Rev.* **B 86**, 054112 (2012).
- [23] Jong-Woo Kim, Paul Thompson, Simon Brown, Peter S. Normile, John A. Schlueter, Andrey Shkabko, Anke Weidenkaff, and Philip J. Ryan. Emergent superstructural dynamic order due to competing antiferroelectric and antiferrodistortive instabilities in bulk EuTiO₃. *Phys. Rev. Lett.* **110**, 027201 (2013)

-
- [24] Ronald Maran, Shintaro Yasui, E.A. Eliseev, M.D. Glinchuk, A.N. Morozovska, Hiroshi Funakubo, Ichiro Takeuchi, Nagarajan Valanoor. Interface control of a morphotropic phase boundary in epitaxial samarium-modified bismuth ferrite superlattices. *Phys.Rev.* **B 90**, 245131 (2014)
- [25] Y.M. Jin, Y.U. Wang, A.G. Khachatryan, J. F. Li and D. Viehland, Adaptive ferroelectric states in systems with low domain wall energy: Tetragonal microdomains. *J. Appl. Phys.* **94**, 3629 (2003).
- [26] Y.M. Jin, Y.U. Wang, A.G. Khachatryan, J. F. Li and D. Viehland. Conformal miniaturization of domains with low domain-wall energy: Monoclinic ferroelectric states near the morphotropic phase boundaries. *Phys. Rev. Lett.* **91**, 197601 (2003).
- [27] Y.U. Wang, Three intrinsic relationships of lattice parameters between intermediate monoclinic M C and tetragonal phases in ferroelectric Pb [(Mg 1/3 Nb 2/3) 1– x Ti x] O 3 and Pb [(Zn 1/3 Nb 2/3) 1– x Ti x] O 3 near morphotropic phase boundaries. *Phys. Rev. B* **73**, 014113 (2006).
- [28] S. Kaufmann, U. K. Roßler, O. Heczko, M. Wuttig, J. Buschbeck, L. Schultz, and S. Fahle. Adaptive modulations of martensites. *Phys. Rev. Lett.* **104**, 145702 (2010).
- [29] A.N. Morozovska, E.A. Eliseev, S.V. Kalinin, L.-Q. Chen and V. Gopalan. Surface polar states and pyroelectricity in ferroelastics induced by flexo-roto field. *Appl. Phys. Lett.* **100**, 142902 (2012).
- [30] A.N. Morozovska, E.A. Eliseev, S.L. Bravina, A.Y. Borisevich, and S.V. Kalinin. Roto-flexoelectric coupling impact on the phase diagrams and pyroelectricity of thin SrTiO₃ films. *J. Appl. Phys.* **112**, 064111 (2012).
- [31] N. A. Pertsev, A. K. Tagantsev, and N. Setter, Phase transitions and strain-induced ferroelectricity in SrTiO₃ epitaxial thin films. *Phys. Rev. B* **61**, R825 (2000).
- [32] A. N. Morozovska, Y. Gu, V. V. Khist, M. D. Glinchuk, L.-Q. Chen, V. Gopalan, and E. A. Eliseev, Low-symmetry monoclinic ferroelectric phase stabilized by oxygen octahedra rotations in strained Eux Sr 1– x TiO₃ thin films. *Phys. Rev. B* **87**, 134102 (2013).
- [33] N.A. Pertsev, A.G. Zembilgotov, A. K. Tagantsev. Effect of Mechanical Boundary Conditions on Phase Diagrams of Epitaxial Ferroelectric Thin Films. *Phys. Rev. Lett.* **80**, 1988 (1998).
- [34] O. Diéguez, S. Tinte, A. Antons, C. Bungaro, J. B. Neaton, K. M. Rabe, and D. Vanderbilt, Ab initio study of the phase diagram of epitaxial BaTiO₃, *Phys. Rev. B* **69**, 212101 (2004).
- [35] Y.L. Li, L. Q. Chen. Temperature-strain phase diagram for Ba Ti O₃ thin films. *Appl. Phys. Lett.* **88**, 072905 (2006).
- [36] A. Gruverman, D. Wu, H-J Fan, I Vrejoiu, M Alexe, R J Harrison and J F Scott, Vortex ferroelectric domains, *J. Phys.: Condens. Matter* **20**, 342201 (2008).
- [37] A. K.Yadav, C. T. Nelson, S. L. Hsu, Z. Hong, J. D. Clarkson, C. M. Schlepütz, A. R. Damodaran, P. Shafer, E. Arenholz, L. R. Dedon, D. Chen, A. Vishwanath, A. M. Minor, L. Q. Chen, J. F. Scott, L. W. Martin, and R. Ramesh, Observation of polar vortices in oxide superlattices, *Nature* **530**, 198 (2016).
- [38] N. Balke, B. Winchester, Wei Ren, Ying Hao Chu, A. N. Morozovska, E. A. Eliseev, M. Huijben, R. K. Vasudevan, P. Maksymovych, J. Britson, S. Jesse, I. Kornev, R. Ramesh, L. Bellaiche, L.-Q. Chen, and S. V. Kalinin,. Enhanced electric conductivity at ferroelectric vortex cores in BiFeO₃, *Nat. Phys.* **8**, 81 (2012).

-
- [39] B. Winchester, N. Balke, X. X. Cheng, A. N. Morozovska, S. Kalinin, and L. Q. Chen, Electroelastic fields in artificially created vortex cores in epitaxial BiFeO₃ thin films, *Appl. Phys. Lett.* 107, 052903 (2015).
- [40] G. Catalan, H. Béa, S. Fusil, M. Bibes, Patrycja Paruch, A. Barthélémy, and J. F. Scott, Fractal dimension and size scaling of domains in thin films of multiferroic BiFeO₃, *Phys. Rev. Lett.* 100, 027602 (2008).
- [41] S. V. Kalinin, B. J. Rodriguez, J. D. Budai, S. Jesse, A. N. Morozovska, A. A. Bokov, and Z. G. Ye, Direct evidence of mesoscopic dynamic heterogeneities at the surfaces of ergodic ferroelectric relaxors, *Phys. Rev. B* 81, 064107 (2010).
- [42] V. V. Shvartsman, and A. L. Kholkin, Domain structure of (Pb (Mg_{1/3}Nb_{2/3})O₃)_{0.8}(PbTiO₃)_{0.2} studied by piezoresponse force microscopy, *Phys. Rev. B* 69, 014102 (2004).
- [43] K. S. Wong, J. Y. Dai, X. Y. Zhao, and H. S. Luo, Time-and temperature-dependent domain evolutions in poled (111)-cut (Pb (Mg_{1/3}Nb_{2/3})O₃)_{0.7} (PbTiO₃)_{0.3} single crystal, *Appl. Physics Lett.* 90, 162907 (2007).
- [44] A. Kholkin, A. Morozovska, D. Kiselev, I. Bdikin, B. Rodriguez, P. Wu, A. Bokov, Z.-G. Ye, B. Dkhil, L.-Q. Chen, M. Kosec, and S. V. Kalinin. Surface Domain Structures and Mesoscopic Phase Transition in Relaxor Ferroelectrics. *Adv. Func. Mat.* 21 (11), 1977 (2011).
- [45] A. N. Morozovska, E. A. Eliseev, J. Wang, G. S. Svechnikov, Yu. M. Vysochanskii, V. Gopalan, and L.-Q. Chen, Phase diagram and domain splitting in thin ferroelectric films with incommensurate phase, *Phys. Rev. B* 81, 195437 (2010).
- [46] A. Artemev, B. Geddes, J. Slutsker, and A. Roytburd, Thermodynamic analysis and phase field modeling of domain structures in bilayer ferroelectric thin films, *J. Appl. Phys.* 103, 074104 (2008).
- [47] A. Hubert, and R. Schafer, *Magnetic domains: the analysis of magnetic microstructures*, (Springer, Berlin 1998).
- [48] E. A. Eliseev, Y. M. Fomichov, S. V. Kalinin, Y. M. Vysochanskii, P. Maksymovich and A. N. Morozovska. Labyrinthine domains in ferroelectric nanoparticles: Manifestation of a gradient-induced morphological phase transition. *Phys.Rev. B* **98**, 054101 (2018).
- [49] Anna N. Morozovska, Yevhen M. Fomichov, Petro Maksymovych, Yulian M. Vysochanskii, and Eugene A. Eliseev. Analytical description of domain morphology and phase diagrams of ferroelectric nanoparticles *Acta Materialia* **160**, 109-120 (2018)
- [50] D.C. Arnold, K.S. Knight, G. Catalan, S.A.T. Redfern, James F. Scott, Philip Lightfoot, and Finlay D. Morrison, The β -to- γ Transition in BiFeO₃: A Powder Neutron Diffraction Study, *Advanced Functional Materials* 20, 2116 (2010).
- [51] R. Palai, R. S. Katiyar, Hans Schmid, Paul Tissot, S. J. Clark, J. Robertson, S. A. T. Redfern, G. A. Catalan, and J. F. Scott, β phase and γ - β metal-insulator transition in multiferroic BiFeO₃, *Phys. Rev. B* 77, 014110 (2008).
- [52] P. Fischer, M. Polomska, I. Sosnowska, M. Szymanski. "Temperature dependence of the crystal and magnetic structures of BiFeO₃." *Journal of Physics C: Solid State Physics* 13, no. 10, 1931 (1980).
- [53] O. Dieguez, P. Aguado-Puente, J. Junquera, J. Iniguez. Domain walls in a perovskite oxide with two primary structural order parameters: First-principles study of BiFeO₃. *Phys. Rev. B* 87, 024102 (2013).

-
- [54] Q. He, C.-H. Yeh, J.-C. Yang, G. Singh-Bhalla, C.-W. Liang, P.-W. Chiu, G. Catalan, L.W. Martin, Y.-H. Chu, J. F. Scott, and R. Ramesh. "Magnetotransport at domain walls in BiFeO₃." *Physical review letters* 108, no. 6: 067203 (2012).
- [55] G. Catalan, J. Seidel, R. Ramesh, and J. F. Scott. "Domain wall nanoelectronics." *Reviews of Modern Physics* 84, no. 1: 119 (2012).
- [56] Nina Balke, Benjamin Winchester, Wei Ren, Ying Hao Chu, Anna N. Morozovska, Eugene A. Eliseev, Mark Huijben, Rama K. Vasudevan, Petro Maksymovych, Jason Britson, Stephen Jesse, Igor Kornev, Ramamoorthy Ramesh, Laurent Bellaiche, Long Qing Chen, and Sergei V. Kalinin.. Enhanced electric conductivity at ferroelectric vortex cores in BiFeO₃. *Nature Physics* 8, 81–88 (2012)
- [57] Anna N. Morozovska, Rama K. Vasudevan, Peter Maksymovych, Sergei V. Kalinin and Eugene A. Eliseev. Anisotropic conductivity of uncharged domain walls in BiFeO₃. *Phys. Rev. B.* **86**, 085315 (2012)
- [58] R. K. Vasudevan, A. N. Morozovska, E. A. Eliseev, J. Britson, J.-C. Yang, Y.-H. Chu, P. Maksymovych, L. Q. Chen, V. Nagarajan, S. V. Kalinin. Domain wall geometry controls conduction in ferroelectrics. *Nano Letters*, 12 (11), pp 5524–5531 (2012)
- [59] R. K. Vasudevan, W. Wu, J. R. Guest, A. P. Baddorf, A. N. Morozovska, E. A. Eliseev, N. Balke, V. Nagarajan, P. Maksymovych. Domain Wall Conduction and Polarization-Mediated Transport in Ferroelectrics. *Adv. Funct. Mater.*, **23**, 2592–2616 (2013)
- [60] D.V. Karpinsky, E.A. Eliseev, Fei Xue, M.V. Silibin, A. Franz, M.D. Glinchuk, I.O. Troyanchuk, S.A. Gavrilov, Venkatraman Gopalan, Long-Qing Chen, and A.N. Morozovska, Thermodynamic potential and phase diagram for multiferroic bismuth ferrite (BiFeO₃), *npj Computational Materials* 3, 20 (2017)
- [61] J. Wang, J. B. Neaton, H. Zheng, V. Nagarajan, S. B. Ogale, B. Liu, D. Viehland, V. Vaithyanathan, D. G. Schlom, U. V. Waghmare, N. A. Spaldin, K. M. Rabe, M. Wuttig, and R. Ramesh, Epitaxial BiFeO₃ multiferroic thin film heterostructures, *Science* 299, 1719 (2003).
- [62] Y.-H. Chu, Qian Zhan, L. W. Martin, M. P. Cruz, Pei-Ling Yang, G.W. Pabst, F. Zavaliche, Seung-Yeul Yang, Jing-Xian Zhang, Long-Qing Chen, D. G. Schlom, I.-Nan Lin, Tai-Bor Wu, and Ramamoorthy Ramesh, Nanoscale domain control in multiferroic BiFeO₃ thin films, *Advanced Materials* 18, 2307 (2006).
- [63] Ying-Hao Chu, L.W. Martin, M.B. Holcomb, M. Gajek, Shu-Jen Han, Qing He, N. Balke, Chan-Ho Yang, Donkoun Lee, Wei Hu, Qian Zhan, Pei-Ling Yang, A. Fraile-Rodríguez, A. Scholl, Shan X. Wang, and Ramamoorthy Ramesh, Electric-field control of local ferromagnetism using a magnetoelectric multiferroic, *Nature materials* 7, 478 (2008).
- [64] P. Maksymovych, M. Huijben, Minghu Pan, S. Jesse, N. Balke, Ying-Hao Chu, Hye Jung Chang, A.Y. Borisevich, A.P. Baddorf, Guus Rijnders, D.H. A. Blank, Ramamoorthy Ramesh, and S.V. Kalinin, Ultrathin limit and dead-layer effects in local polarization switching of BiFeO₃, *Phys. Rev. B*, 85, 014119 (2012).
- [65] C. Beekman, W. Siemons, M. Chi, N. Balke, J. Y. Howe, T. Z. Ward, P. Maksymovych, J. D. Budai, J. Z. Tischler, R. Xu, W. Liu, and H. M. Christen, Ferroelectric Self-Poling, Switching, and Monoclinic Domain Configuration in BiFeO₃ Thin Films, *Advanced Functional Materials* 26, 5166 (2016).

-
- [66] M. Trassin, G. De Luca, S. Manz, and M. Fiebig, Probing ferroelectric domain engineering in BiFeO₃ thin films by second harmonic generation, *Advanced Materials* 27, 4871 (2015).
- [67] W. Y. Wang, Y. L. Tang, Y. L. Zhu, Y. B. Xu, Y. Liu, Y. J. Wang, S. Jagadeesh, X. L. Ma, Atomic Level 1D Structural Modulations at the Negatively Charged Domain Walls in BiFeO₃ Films, *Advanced Materials Interfaces*, 2 (9): 1500024 (2015)
- [68] W. Y. Wang, Y. L. Zhu, Y. L. Tang, Y. B. Xu, Y. Liu, S. Li, S. R. Zhang, Y. J. Wang, X. L. Ma, Large Scale Arrays of Four-State Vortex Domains in BiFeO₃ Thin Film, *Applied Physics Letters*, 109 (20): 202904 (2016).
- [69] Johanna Nordlander, Gabriele De Luca, Nives Strkalj, Manfred Fiebig, and Morgan Trassin. "Probing Ferroic States in Oxide Thin Films Using Optical Second Harmonic Generation." *Applied Sciences* 8, no. 4 570 (2018).
- [70] W. Y. Wang, Y. L. Zhu, Y. L. Tang, M. J. Han, Y. J. Wang, X. L. Ma, Atomic Mapping of Structural Distortions in 109 Degrees Domain Patterned BiFeO₃ Thin Films, *Journal of Materials Research*, 32 (12): 2423-2430 (2017).
- [71] M. J. Han, Y. J. Wang, D. S. Ma, Y. L. Zhu, Y. L. Tang, Y. Liu, N. B. Zhang, J. Y. Ma, X. L. Ma, Coexistence of Rhombohedral and Orthorhombic Phases in Ultrathin BiFeO₃ Films Driven by Interfacial Oxygen Octahedral Coupling, *Acta Materialia*, 145: 220-226 (2018)
- [72] E.A. Eliseev, M.D. Glinchuk, Venkatraman Gopalan, and A.N. Morozovska, Rotomagnetic couplings influence on the magnetic properties of antiferrodistortive antiferromagnets, *J. Appl. Phys.* 118, 144101 (2015)
- [73] Anna N. Morozovska, Eugene A. Eliseev, Maya D. Glinchuk, Olena M. Fesenko, Vladimir V. Shvartsman, Venkatraman Gopalan, Maxim V. Silibin, Dmitry V. Karpinsky. Rotomagnetic coupling in fine-grained multiferroic BiFeO₃: theory and experiment. *Phys. Rev. B* 97, 134115 (2018)
- [74] John H. Barrett, "Dielectric constant in perovskite type crystals." *Physical Review* 86, 118 (1952).
- [75] Yijia Gu, Karin Rabe, Eric Bousquet, Venkatraman Gopalan, and Long-Qing Chen. "Phenomenological thermodynamic potential for CaTiO₃ single crystals." *Physical Review B* 85, no. 6: 064117 (2012).
- [76] J. Bardeen, "Surface states and rectification at a metal semi-conductor contact." *Phys. Rev.* 71 (1947) 717.
- [77] M. J. Highland, T. T. Fister, D. D. Fong, P. H. Fuoss, Carol Thompson, J. A. Eastman, S. K. Streiffer, and G. B. Stephenson. Equilibrium polarization of ultrathin PbTiO₃ with surface compensation controlled by oxygen partial pressure. *Physical Review Letters*, 107, no. 18, (2011) 187602.
- [78] G.B. Stephenson, and M.J. Highland, Equilibrium and stability of polarization in ultrathin ferroelectric films with ionic surface compensation. *Physical Review B*, 84 (6), (2011) 064107
- [79] Sergei V. Kalinin, Yunseok Kim, Dillon Fong, and Anna Morozovska, Surface-screening mechanisms in ferroelectric thin films and their effect on polarization dynamics and domain structures, *Reports on Progress in Physics* 81, (2018) 036502.

-
- [80] Anna N. Morozovska, Eugene A. Eliseev, Ivan S. Vorotiahin, Maxim V. Silibin, Sergei V. Kalinin and Nicholas V. Morozovsky. Control of polarization hysteresis temperature behavior by surface screening in thin ferroelectric films. *Acta Materialia* **160**, 57-71 (2018)
- [81]. E.A. Eliseev, A.V. Semchenko, Y.M. Fomichov, M.D. Glinchuk, V.V. Sidsky, V.V. Kolos, Yu.M. Pleskachevsky, M.V. Silibin, N.V. Morozovsky, A.N. Morozovska. "Surface and finite size effects impact on the phase diagrams, polar and dielectric properties of (Sr,Bi)Ta₂O₉ ferroelectric nanoparticles". *J. Appl. Phys.* **119** 204104 (2016).
- [82] A. K. Tagantsev, G. Gerra, and N. Setter, Short-range and long-range contributions to the size effect in metal-ferroelectric-metal heterostructures. *Phys. Rev. B* **77**, 174111 (2008).
- [83] J. Wang, A. K. Tagantsev, N. Setter. Size effect in ferroelectrics: Competition between geometrical and crystalline symmetries. *Phys. Rev. B* **83**, 014104 (2011)
- [84] L.D. Landau and E.M. Lifshitz, *Theory of Elasticity. Theoretical Physics*, Vol. 7 (Butterworth-Heinemann, Oxford, 1976).
- [85] Igor Dzyaloshinsky, "A thermodynamic theory of "weak" ferromagnetism of antiferromagnetics." *Journal of Physics and Chemistry of Solids* 4, no. 4: 241-255 (1958).
- [86] S.V. Kalinin, A.N. Morozovska, Long Qing Chen, Brian J. Rodriguez. Local polarization dynamics in ferroelectric materials. *Rep. Prog. Phys.* 73, 056502-1-67 (2010).
- [87] Sergio Conti, Stefan Muller, Arkady Poliakovsky, and Ekhard K. H. Salje, Coupling of order parameters, chirality, and interfacial structures in multiferroic materials, *J. Phys.: Condens. Matter* 23 142203 (2011).

SUPPLEMENTARY MATERIALS

APPENDIX A

Evident form of the free energy of antiferrodistortive ferroelectric media

Evident forms of different contributions to the free energy for cubic symmetry aristo-phase are presented below. Contribution of antiferrodistortive (AFD) phase with order parameter Φ_i (vector of tilt of oxygen octahedral groups with components $i=1, 2, 3$) is:

$$\begin{aligned} \Delta G_{AFD} = & b_1(\Phi_1^2 + \Phi_2^2 + \Phi_3^2) + b_{11}(\Phi_1^4 + \Phi_2^4 + \Phi_3^4) + b_{12}(\Phi_1^2\Phi_2^2 + \Phi_1^2\Phi_3^2 + \Phi_3^2\Phi_2^2) + \\ & b_{111}(\Phi_1^6 + \Phi_2^6 + \Phi_3^6) + b_{112}(\Phi_1^2(\Phi_2^4 + \Phi_3^4) + \Phi_1^4(\Phi_2^2 + \Phi_3^2) + \Phi_2^2\Phi_3^4 + \Phi_2^4\Phi_3^2) + b_{123}\Phi_1^2\Phi_2^2\Phi_3^2 + \\ & + v_{11}\left(\left(\frac{\partial\Phi_1}{\partial x_1}\right)^2 + \left(\frac{\partial\Phi_2}{\partial x_2}\right)^2 + \left(\frac{\partial\Phi_3}{\partial x_3}\right)^2\right) + v_{12}\left(\frac{\partial\Phi_1}{\partial x_1}\frac{\partial\Phi_2}{\partial x_2} + \frac{\partial\Phi_2}{\partial x_2}\frac{\partial\Phi_3}{\partial x_3} + \frac{\partial\Phi_1}{\partial x_1}\frac{\partial\Phi_3}{\partial x_3}\right) + \\ & v_{44}\left(\left(\frac{\partial\Phi_1}{\partial x_2}\right)^2 + \left(\frac{\partial\Phi_1}{\partial x_3}\right)^2 + \left(\frac{\partial\Phi_2}{\partial x_1}\right)^2 + \left(\frac{\partial\Phi_2}{\partial x_3}\right)^2 + \left(\frac{\partial\Phi_3}{\partial x_1}\right)^2 + \left(\frac{\partial\Phi_3}{\partial x_2}\right)^2\right) + \\ & + v'_{44}\left(\frac{\partial\Phi_1}{\partial x_2}\frac{\partial\Phi_2}{\partial x_1} + \frac{\partial\Phi_1}{\partial x_3}\frac{\partial\Phi_3}{\partial x_1} + \frac{\partial\Phi_2}{\partial x_3}\frac{\partial\Phi_3}{\partial x_2}\right) \end{aligned} \quad (A.1)$$

Contribution of polarization P_i vector (with three components for $i=1, 2, 3$):

$$\begin{aligned} \Delta G_{FE} = & a_1(P_1^2 + P_2^2 + P_3^2) + a_{11}(P_1^4 + P_2^4 + P_3^4) + a_{12}(P_1^2P_2^2 + P_1^2P_3^2 + P_2^2P_3^2) \\ & + a_{111}(P_1^6 + P_2^6 + P_3^6) + a_{112}(P_1^2(P_2^4 + P_3^4) + P_1^4(P_2^2 + P_3^2) + P_2^2P_3^4 + P_2^4P_3^2) + a_{123}P_1^2P_2^2P_3^2 \\ & + g_{11}\left(\left(\frac{\partial P_1}{\partial x_1}\right)^2 + \left(\frac{\partial P_2}{\partial x_2}\right)^2 + \left(\frac{\partial P_3}{\partial x_3}\right)^2\right) + g_{12}\left(\frac{\partial P_1}{\partial x_1}\frac{\partial P_2}{\partial x_2} + \frac{\partial P_2}{\partial x_2}\frac{\partial P_3}{\partial x_3} + \frac{\partial P_1}{\partial x_1}\frac{\partial P_3}{\partial x_3}\right) + \\ & + g_{44}\left(\left(\frac{\partial P_1}{\partial x_2}\right)^2 + \left(\frac{\partial P_1}{\partial x_3}\right)^2 + \left(\frac{\partial P_2}{\partial x_1}\right)^2 + \left(\frac{\partial P_2}{\partial x_3}\right)^2 + \left(\frac{\partial P_3}{\partial x_1}\right)^2 + \left(\frac{\partial P_3}{\partial x_2}\right)^2\right) + \\ & + g'_{44}\left(\frac{\partial P_1}{\partial x_2}\frac{\partial P_2}{\partial x_1} + \frac{\partial P_1}{\partial x_3}\frac{\partial P_3}{\partial x_1} + \frac{\partial P_2}{\partial x_3}\frac{\partial P_3}{\partial x_2}\right) \end{aligned} \quad (A.2)$$

Contribution for the coupling between polarization and tilt

$$\begin{aligned} \Delta G_{BQC} = & \zeta_{11}(\Phi_1^2P_1^2 + \Phi_2^2P_2^2 + \Phi_3^2P_3^2) + \zeta_{12}((\Phi_2^2 + \Phi_3^2)P_1^2 + (\Phi_1^2 + \Phi_3^2)P_2^2 + (\Phi_1^2 + \Phi_2^2)P_3^2) \\ & + \zeta_{44}(\Phi_1\Phi_2P_1P_2 + \Phi_1\Phi_3P_1P_3 + \Phi_2\Phi_3P_2P_3) \end{aligned} \quad (A.3)$$

Electrostriction and rotostriction contributions to the free energy are

$$\begin{aligned} \Delta G_{striction} = & -Q_{11}(\sigma_{11}P_1^2 + \sigma_{22}P_2^2 + \sigma_{33}P_3^2) \\ & -Q_{12}((\sigma_{22} + \sigma_{33})P_1^2 + (\sigma_{11} + \sigma_{33})P_2^2 + (\sigma_{22} + \sigma_{11})P_3^2) \\ & -Q_{44}(\sigma_{12}P_1P_2 + \sigma_{13}P_1P_3 + \sigma_{23}P_2P_3) \\ & -R_{11}(\sigma_{11}\Phi_1^2 + \sigma_{22}\Phi_2^2 + \sigma_{33}\Phi_3^2) - R_{12}((\sigma_{22} + \sigma_{33})\Phi_1^2 + (\sigma_{11} + \sigma_{33})\Phi_2^2 + (\sigma_{22} + \sigma_{11})\Phi_3^2) \\ & -R_{44}(\sigma_{12}\Phi_1\Phi_2 + \Phi_1\Phi_3 + \sigma_{23}\Phi_2\Phi_3) \end{aligned} \quad (A.4)$$

Flexoelectric effect contribution is

$$\begin{aligned}\Delta G_{\text{flexo}} = & -F_{11} \left(\sigma_{11} \frac{\partial P_1}{\partial x_1} + \sigma_{22} \frac{\partial P_2}{\partial x_2} + \sigma_{33} \frac{\partial P_3}{\partial x_3} \right) \\ & - F_{12} \left((\sigma_{22} + \sigma_{33}) \frac{\partial P_1}{\partial x_1} + (\sigma_{11} + \sigma_{33}) \frac{\partial P_2}{\partial x_2} + (\sigma_{11} + \sigma_{22}) \frac{\partial P_3}{\partial x_3} \right) \\ & - F_{44} \left(\sigma_{12} \left(\frac{\partial P_1}{\partial x_2} + \frac{\partial P_2}{\partial x_1} \right) + \sigma_{13} \left(\frac{\partial P_1}{\partial x_3} + \frac{\partial P_3}{\partial x_1} \right) + \sigma_{23} \left(\frac{\partial P_2}{\partial x_3} + \frac{\partial P_3}{\partial x_2} \right) \right)\end{aligned}\quad (\text{A.5})$$

Elastic "self-energy" is

$$\Delta G_{\text{elast}} = -\frac{S_{11}}{2} (\sigma_{11}^2 + \sigma_{22}^2 + \sigma_{33}^2) - s_{12} (\sigma_{11}\sigma_{22} + \sigma_{22}\sigma_{33} + \sigma_{11}\sigma_{33}) - \frac{S_{44}}{2} (\sigma_{12}^2 + \sigma_{23}^2 + \sigma_{13}^2) \quad (\text{A.6})$$

Total free energy density has the following form

$$G = \Delta G_{AFD} + \Delta G_{FE} + \Delta G_{BQC} + \Delta G_{striction} + \Delta G_{flexo} + \Delta G_{elast} \quad (\text{A.7})$$

The Euler-Lagrange equations of LGD theory for polarization P_i and tilt Φ_i components ($i=1, 2, 3$) could be obtained by the minimization of the free energy (A.7) as follows

$$\begin{aligned}& 2P_1(a_1 - Q_{12}(\sigma_{22} + \sigma_{33}) - Q_{11}\sigma_{11}) - Q_{44}(\sigma_{12}P_2 + \sigma_{13}P_3) + (\zeta_{11}\Phi_1^2 + \zeta_{12}(\Phi_2^2 + \Phi_3^2))2P_1 + \zeta_{44}\Phi_1(\Phi_2P_2 + \Phi_3P_3) \\ & + 4a_{11}P_1^3 + 2a_{12}P_1(P_2^2 + P_3^2) + 6a_{111}P_1^5 + 2a_{112}P_1(P_2^4 + 2P_1^2P_2^2 + P_3^4 + 2P_1^2P_3^2) + 2a_{112}P_1P_2^2P_3^2 \\ & - g_{11}\frac{\partial^2 P_1}{\partial x_1^2} - g_{44}\left(\frac{\partial^2 P_1}{\partial x_2^2} + \frac{\partial^2 P_1}{\partial x_3^2}\right) - (g'_{44} + g_{12})\frac{\partial^2 P_2}{\partial x_2\partial x_1} - (g'_{44} + g_{12})\frac{\partial^2 P_3}{\partial x_3\partial x_1} \\ & + F_{11}\frac{\partial\sigma_{11}}{\partial x_1} + F_{12}\left(\frac{\partial\sigma_{22}}{\partial x_1} + \frac{\partial\sigma_{33}}{\partial x_1}\right) + F_{44}\left(\frac{\partial\sigma_{12}}{\partial x_2} + \frac{\partial\sigma_{13}}{\partial x_3}\right) = E_1\end{aligned}\quad (\text{A.8a})$$

$$\begin{aligned}& 2P_2(a_1 - Q_{12}(\sigma_{11} + \sigma_{33}) - Q_{11}\sigma_{22}) - Q_{44}(\sigma_{12}P_1 + \sigma_{23}P_3) + (\zeta_{11}\Phi_2^2 + \zeta_{12}(\Phi_1^2 + \Phi_3^2))2P_2 + \zeta_{44}\Phi_2(\Phi_1P_1 + \Phi_3P_3) \\ & + 4a_{11}P_2^3 + 2a_{12}P_2(P_1^2 + P_3^2) + 6a_{111}P_2^5 + 2a_{112}P_2(P_1^4 + 2P_2^2P_1^2 + P_3^4 + 2P_2^2P_3^2) + 2a_{112}P_2P_1^2P_3^2 \\ & - g_{11}\frac{\partial^2 P_2}{\partial x_2^2} - g_{44}\left(\frac{\partial^2 P_2}{\partial x_1^2} + \frac{\partial^2 P_2}{\partial x_3^2}\right) - (g'_{44} + g_{12})\frac{\partial^2 P_1}{\partial x_2\partial x_1} - (g'_{44} + g_{12})\frac{\partial^2 P_3}{\partial x_3\partial x_2} \\ & + F_{11}\frac{\partial\sigma_{22}}{\partial x_2} + F_{12}\left(\frac{\partial\sigma_{11}}{\partial x_2} + \frac{\partial\sigma_{33}}{\partial x_2}\right) + F_{44}\left(\frac{\partial\sigma_{12}}{\partial x_1} + \frac{\partial\sigma_{23}}{\partial x_3}\right) = E_2\end{aligned}\quad (\text{A.8b})$$

$$\begin{aligned}& 2P_3(a_1 - Q_{12}(\sigma_{11} + \sigma_{22}) - Q_{11}\sigma_{33}) - Q_{44}(\sigma_{13}P_1 + \sigma_{23}P_2) + (\zeta_{11}\Phi_3^2 + \zeta_{12}(\Phi_1^2 + \Phi_2^2))2P_3 + \zeta_{44}\Phi_3(\Phi_1P_1 + \Phi_2P_2) \\ & + 4a_{11}P_3^3 + 2a_{12}P_3(P_1^2 + P_2^2) + 6a_{111}P_3^5 + 2a_{112}P_3(P_1^4 + 2P_3^2P_1^2 + P_2^4 + 2P_3^2P_2^2) + 2a_{112}P_3P_1^2P_2^2 \\ & - g_{11}\frac{\partial^2 P_3}{\partial x_3^2} - g_{44}\left(\frac{\partial^2 P_3}{\partial x_1^2} + \frac{\partial^2 P_3}{\partial x_2^2}\right) - (g'_{44} + g_{12})\frac{\partial^2 P_1}{\partial x_3\partial x_1} - (g'_{44} + g_{12})\frac{\partial^2 P_2}{\partial x_3\partial x_2} \\ & + F_{11}\frac{\partial\sigma_{33}}{\partial x_3} + F_{12}\left(\frac{\partial\sigma_{11}}{\partial x_3} + \frac{\partial\sigma_{33}}{\partial x_3}\right) + F_{44}\left(\frac{\partial\sigma_{13}}{\partial x_1} + \frac{\partial\sigma_{23}}{\partial x_2}\right) = E_3\end{aligned}\quad (\text{A.8c})$$

$$\begin{aligned}
& (b_1 - R_{12}(\sigma_{22} + \sigma_{33}) - R_{11}\sigma_{11} + \zeta_{11}P_1^2 + \zeta_{12}(P_2^2 + P_3^2))2\Phi_1 - R_{44}(\sigma_{12}\Phi_2 + \sigma_{13}\Phi_3) + \zeta_{44}P_1(\Phi_2P_2 + \Phi_3P_3) \\
& + 4b_{11}\Phi_1^3 + 2b_{12}\Phi_1(\Phi_2^2 + \Phi_3^2) + 6b_{111}\Phi_1^5 + 2b_{112}\Phi_1(\Phi_2^4 + 2\Phi_1^2\Phi_2^2 + \Phi_3^4 + 2\Phi_1^2\Phi_3^2) + 2b_{112}\Phi_1\Phi_2^2\Phi_3^2 \quad (\text{A.9a}) \\
& - v_{11}\frac{\partial^2\Phi_1}{\partial x_1^2} - v_{44}\left(\frac{\partial^2\Phi_1}{\partial x_2^2} + \frac{\partial^2\Phi_1}{\partial x_3^2}\right) - (v'_{44} + v_{12})\frac{\partial^2\Phi_2}{\partial x_1\partial x_2} - (v'_{44} + v_{12})\frac{\partial^2\Phi_3}{\partial x_1\partial x_3} = 0
\end{aligned}$$

$$\begin{aligned}
& (b_1 - R_{12}(\sigma_{11} + \sigma_{33}) - R_{11}\sigma_{22} + \zeta_{11}P_2^2 + \zeta_{12}(P_1^2 + P_3^2))2\Phi_2 - R_{44}(\sigma_{12}\Phi_1 + \sigma_{23}\Phi_3) + \zeta_{44}P_2(\Phi_1P_1 + \Phi_3P_3) \\
& + 4b_{11}\Phi_2^3 + 2b_{12}\Phi_2(\Phi_1^2 + \Phi_3^2) + 6b_{111}\Phi_2^5 + 2b_{112}\Phi_2(\Phi_1^4 + 2\Phi_1^2\Phi_2^2 + \Phi_3^4 + 2\Phi_2^2\Phi_3^2) + 2b_{112}\Phi_2\Phi_1^2\Phi_3^2 \quad (\text{A.9b}) \\
& - v_{11}\frac{\partial^2\Phi_2}{\partial x_2^2} - v_{44}\left(\frac{\partial^2\Phi_2}{\partial x_1^2} + \frac{\partial^2\Phi_2}{\partial x_3^2}\right) - (v'_{44} + v_{12})\frac{\partial^2\Phi_1}{\partial x_1\partial x_2} - (v'_{44} + v_{12})\frac{\partial^2\Phi_3}{\partial x_2\partial x_3} = 0
\end{aligned}$$

$$\begin{aligned}
& (b_1 - R_{12}(\sigma_{22} + \sigma_{11}) - R_{11}\sigma_{33} + \zeta_{11}P_3^2 + \zeta_{12}(P_2^2 + P_1^2))2\Phi_3 - R_{44}(\sigma_{23}\Phi_2 + \sigma_{13}\Phi_1) + \zeta_{44}P_3(\Phi_2P_2 + \Phi_1P_1) \\
& + 4b_{11}\Phi_3^3 + 2b_{12}\Phi_3(\Phi_1^2 + \Phi_2^2) + 6b_{111}\Phi_3^5 + 2b_{112}\Phi_3(\Phi_2^4 + 2\Phi_3^2\Phi_2^2 + \Phi_1^4 + 2\Phi_1^2\Phi_3^2) + 2b_{112}\Phi_3\Phi_1^2\Phi_2^2 \quad (\text{A.9c}) \\
& - v_{11}\frac{\partial^2\Phi_3}{\partial x_3^2} - v_{44}\left(\frac{\partial^2\Phi_3}{\partial x_2^2} + \frac{\partial^2\Phi_3}{\partial x_1^2}\right) - (v'_{44} + v_{12})\frac{\partial^2\Phi_1}{\partial x_1\partial x_3} - (v'_{44} + v_{12})\frac{\partial^2\Phi_2}{\partial x_2\partial x_3} = 0
\end{aligned}$$

The boundary conditions without flexoelectric effect

$$b^{(S)}\Phi_i + v_{ijkl}\frac{\partial\Phi_k}{\partial x_l}n_j \Big|_S = 0, \quad a^{(P)}P_i + g_{ijkl}\frac{\partial P_k}{\partial x_l}n_j \Big|_S = 0 \quad (i=1, 2, 3) \quad (\text{A.10})$$

For the normal $n_l = \{0, 0, \pm 1\}$ to the surface $x_3 = 0, h$ have the following explicit form

$$\begin{aligned}
b^{(S)}\Phi_1 \mp \left(v_{44}\frac{\partial\Phi_1}{\partial x_3} + v'_{44}\frac{\partial\Phi_3}{\partial x_1} \right) \Big|_{x_3=0,h} &= 0, \quad b^{(S)}\Phi_2 \mp \left(v_{44}\frac{\partial\Phi_2}{\partial x_3} + v'_{44}\frac{\partial\Phi_3}{\partial x_2} \right) \Big|_{x_3=0,h} = 0, \\
b^{(S)}\Phi_3 \mp \left(v_{11}\frac{\partial\Phi_3}{\partial x_3} + v_{12}\frac{\partial\Phi_2}{\partial x_2} + v_{12}\frac{\partial\Phi_1}{\partial x_1} \right) \Big|_{x_3=0,h} &= 0 \quad (\text{A.11a})
\end{aligned}$$

$$\begin{aligned}
a^{(S)}P_1 \mp \left(g_{44}\frac{\partial P_1}{\partial x_3} + g'_{44}\frac{\partial P_3}{\partial x_1} \right) \Big|_{x_3=0,h} &= 0, \quad a^{(S)}P_2 \mp \left(g_{44}\frac{\partial P_2}{\partial x_3} + g'_{44}\frac{\partial P_3}{\partial x_2} \right) \Big|_{x_3=0,h} = 0, \\
a^{(S)}P_3 \mp \left(g_{11}\frac{\partial P_3}{\partial x_3} + g_{12}\frac{\partial P_2}{\partial x_2} + g_{12}\frac{\partial P_1}{\partial x_1} \right) \Big|_{x_3=0,h} &= 0 \quad (\text{A.11b})
\end{aligned}$$

Note that all derivatives $\frac{\partial}{\partial x_2}$ are zero for the 2D-problem. Note that following Glinka and Marton semi-

microscopic model, we suggested that

$$g'_{44} + g_{12} \equiv 0 \quad \text{and} \quad v'_{44} + v_{12} \equiv 0 \quad (\text{A.12})$$

APPENDIX B. Supplementary figures

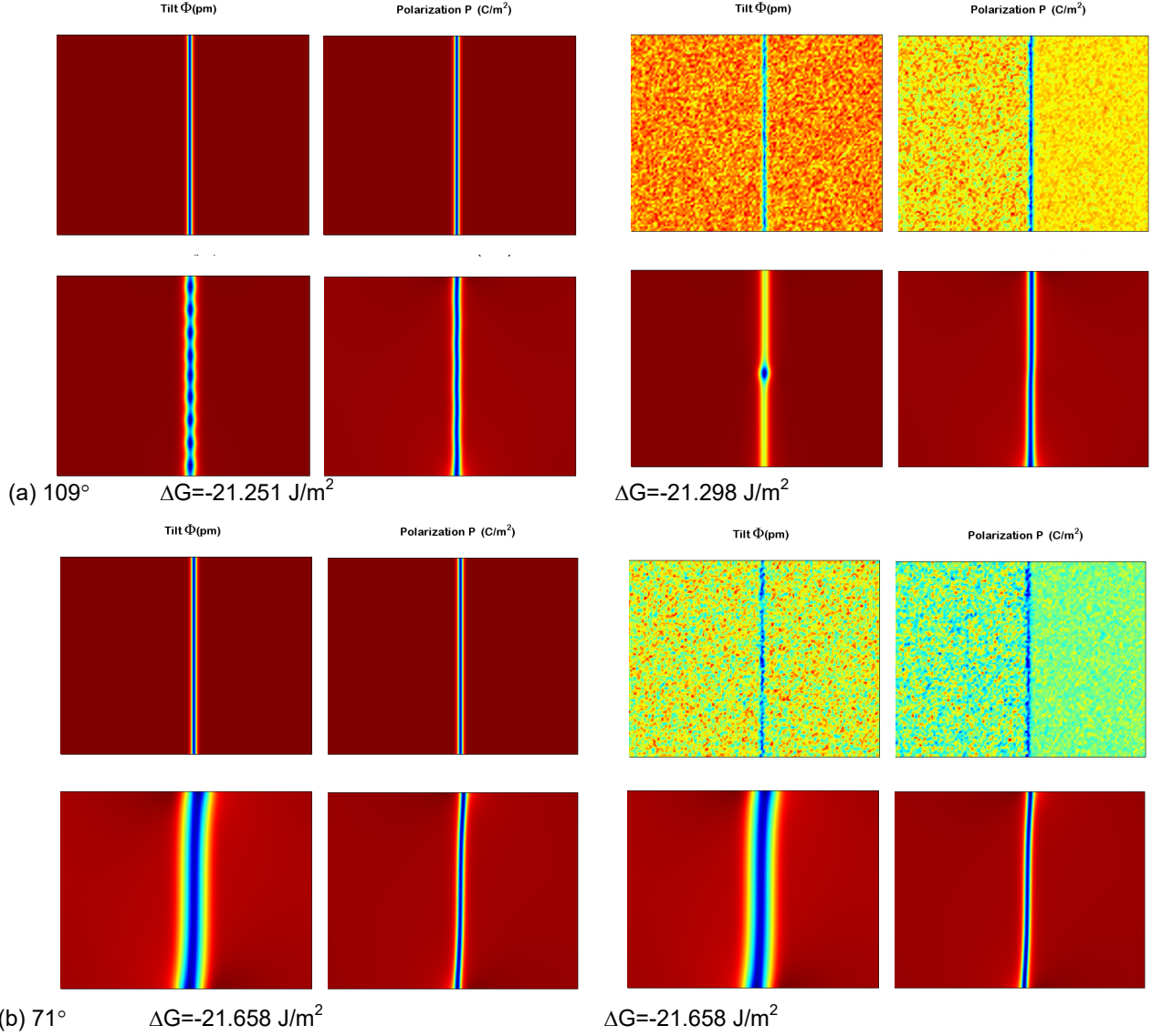


FIGURE. S1. Initial and final distributions of the tilt (**a, c**) and polarization (**b,d**) in a 16-nm BFO film at room temperature for the 109- and 71-degree domains random seeding. Gradient coefficient $\nu_{44} = 0.25 \times 10^{11} \text{ J/m}^3$, $\Lambda = 0$, other parameters of BFO are listed in **Table I**.

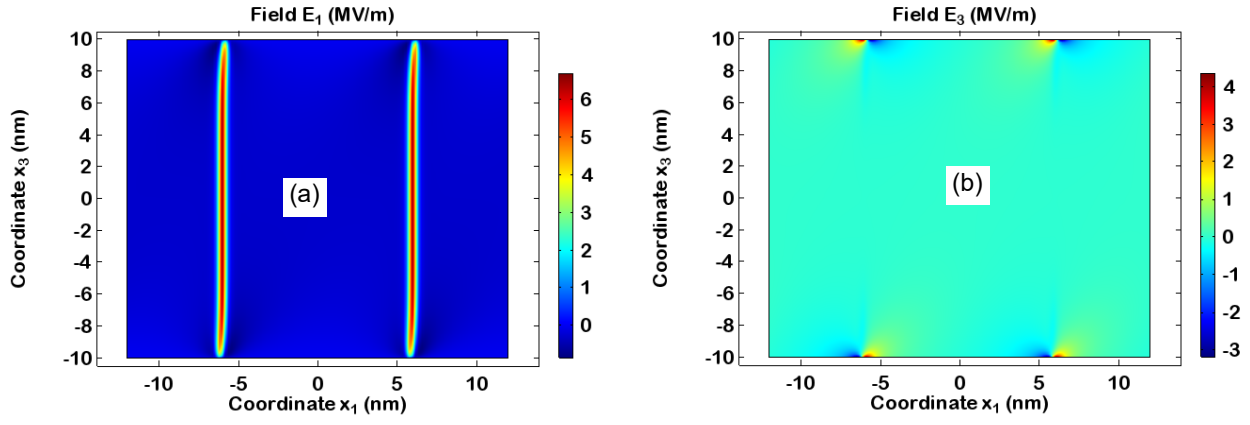


FIGURE S2. Distribution of different components of the electric field, E_1 **(a)** and E_3 **(b)** in a thin BFO film at room temperature for the case of 71° -domains with $[100]$ walls. Gradient coefficient $\nu_{44}=0.25 \times 10^{11}$ J/ m³, other LGD parameters are listed in **Table I**.